$N\!A\!S\!A\!-\!C\!R\!-\!174,702$

NASA
National Aeronautics and
Space Administration

ROCKET INJECTOR ANOMALIES STUDY

Volume I: Description of the Mathematical Model and Solution Procedure

by

A.J. Przekwas, A.K. Singhal and L.T. Tam

CHAM of North America, Incorporated

August 1984

Prepared for

NATIONAL AERONAUTICS AND SPACE ADMINISTRATION
NASA-Lewis Research Center
Contract NAS3-23352

11   1   1 RN/NASA-CR-174702
          DISPLAY 11/2/1
     84N32428*#   ISSUE 22   PAGE 3543   CATEGORY 20   RPT#: NASA-CR-174702 NAS
     1.26:174702 CHAM-H3605/15-VOL-1   CNT#: NAS3-23352   84/08/00   2 VOLS   95
     PAGES   UNCLASSIFIED DOCUMENT
UTTL: Rocket injector anomalies study. Volume 1: Description of the
      mathematical model and solution procedure   TLSP: Final Report
AUTH: A/PRZEKWAS, A. J.; B/SINGHAL, A. K.; C/TAM, L. T.
CORP: CHAM of North America, Inc., Huntsville, Ala.   AVAIL.NTIS   SAP: HC
      A05/MF A01
MAJS: /*COMBUSTION CHAMBERS/*MATHEMATICAL MODELS/*PROPULSION SYSTEM
      CONFIGURATIONS/*ROCKET ENGINES
MINS: / COMBUSTION EFFICIENCY/ COMPUTER PROGRAMS/ EULER-LAGRANGE EQUATION/
      TURBULENT FLOW
ABA: E.A.K.
ABS: The capability of simulating three dimensional two phase reactive flows
     with combustion in the liquid fuelled rocket engines is demonstrated. This
     was accomplished by modifying an existing three dimensional computer
     program (REFLAN3D) with Eulerian Lagrangian approach to simulate two phase
     spray flow, evaporation and combustion. The modified code is referred as
     REFLAN3D-SPRAY. The mathematical formulation of the fluid flow, heat
     transfer, combustion and two phase flow interaction of the numerical
     solution procedure, boundary conditions and their treatment are described.

ENTER:

1. Report No. CR-174702	2. Government Accession No.	3. Recipient's Catalog No.
4. Title and Subtitle Rocket Injector Anomalies Study. Description of the Mathematical Model and Solution procedure		5. Report Date July 1984
		6. Performing Organization Code
7. Author(s) A.J. Przekwas, A.K. Singhal, and L.T. Tam		8. Performing Organization Report No. H3605/15
		10. Work Unit No.
9. Performing Organization Name and Address CHAM of North America Incorporated 1525-A Sparkman DRive Huntsville, Alabama 35805		11. Contract or Grant No. NAS3-23352
12. Sponsoring Agency Name and Address NASA - Lewis Research Center		13. Type of Report and Period Covered Final
		14. Sponsoring Agency Code

15. Supplementary Notes

Project Manager: Dr. Larry P. Cooper
NASA Lewis Research Center
21000 Brookpark Road
Cleveland, Ohio 44135

16. Abstract

The objective of the project was to demonstrate the capability of simulating three-dimensional two-phase reactive flows with combustion in the liquid fuelled rocket engines. This has been accomplished by modifying an existing three-dimensional computer program (REFLAN3D) with Eulerian - Lagrangian approach for simulating two-phase spray flow, evaporation and combustion. The modified code is referred as REFLAN3D-SPRAY.

The report describes the mathematical formulation of the fluid flow, heat transfer, combustion and two-phase flow interaction. It also includes description of the numerical solution procedure, boundary conditions and their treatment. Results of the parametric studies are described in an accompanying report NASA CR 174703.

17. Key Words (Suggested by Author(s)) Rocket Engines, Propulsion, Combustor Models, Spray Combustion and Turbulent flow.	18. Distribution Statement

19. Security Classif. (of this report) UNCLASSIFIED	20. Security Classif. (of this page) UNCLASSIFIED	21. No. of pages 92	22. Price*

N84-32428#

FOREWORD

CHAM of North America Incorporated has performed a Rocket Injector Anomaly Study under the NASA Contract NAS3-23352.

The purpose of the study was to modify, test and demonstrate a computer code for predicting three-dimensional two-phase spray flow and combustion in rocket engines. The modified computer code REFLAN3D-SPRAY (REactive FLow ANalyzer 3-Dimensional, with two-phase spray) and results of parametric studies have been described in the following two volumes:

> Volume 1: Description of the Mathematical Model and
> Solution Procedure; and
> Volume 2: Results of Parametric Studies.

Transfer of the code to NASA LeRC computer center, and preparation of a user's manual are recommended as next steps of the study.

The authors wish to thank all those who have contributed to this work. In particular, thanks are due to Larry P. Cooper and Ken Davidian of the Communications and Propulsion Section of NASA LeRC; and to Laurence Keeton, Jack Keck, Kelli King, Janet Siersma, and Ronni Rossic of CHAM NA.

TABLE OF CONTENTS

1.   SUMMARY

The liquid fuelled rocket engine combustors consist of an injector plate
and a thrust chamber. The injector plate consists of a number of propellant
injectors which are designed to atomize the liquid jets of reactants
and to promote intensive mixing between the vaporized components.

Figure 1.1 shows the schematic of the rocket engine and injector plate,
with LOX-RP1-LOX unlike triplet injectors, considered. The purpose of
the study was to demonstrate an analytical capability to predict the
effects of reactant injection non uniformities (injection anomalies) on
heat transfer to the walls. For this purpose an existing three-dimensional
single-phase flow and combustion computer code (REFLAN3D: - REactive FLow
ANalyzer, 3-Dimensional) has been modified for simulating two-phase flows
in liquid propellant rocket engines. The modified code is referred to as
REFLAN3D-SPRAY.

The numerical model in the final code assumes instantaneous evaporation of
oxygen jets and treats fuel drops as discrete drops of given size spectrum.
It accounts for the liquid fuel (kerosene) jet motion, evaporation, its
interaction with the gaseous phase, and combustion.

The coupling between the liquid jets and the gas-phase includes:

-   momentum interaction between the high speed liquid jets and
    gas phase;
-   energy interaction between hot reacting gases and cold evaporating
    jets; and
-   mass transfer between the evaporating jets and gas phase.

The velocity slip between the liquid drops and the reacting gases is of
primary importance for accurate predictions of flow and heat-transfer
characteristics.

The Eulerian-Lagrangean approach for simulating spray flow, evaporation and
combustion has been selected. A nonorthogonal body fitted coordinate
system is employed for accurate simulation of combustor geometry and near-
wall processes.

Injector Plate

Injector Detail

60°

LOX

RP1

Z

R

Flow

2.60"
Dia

3.00"

17.00"
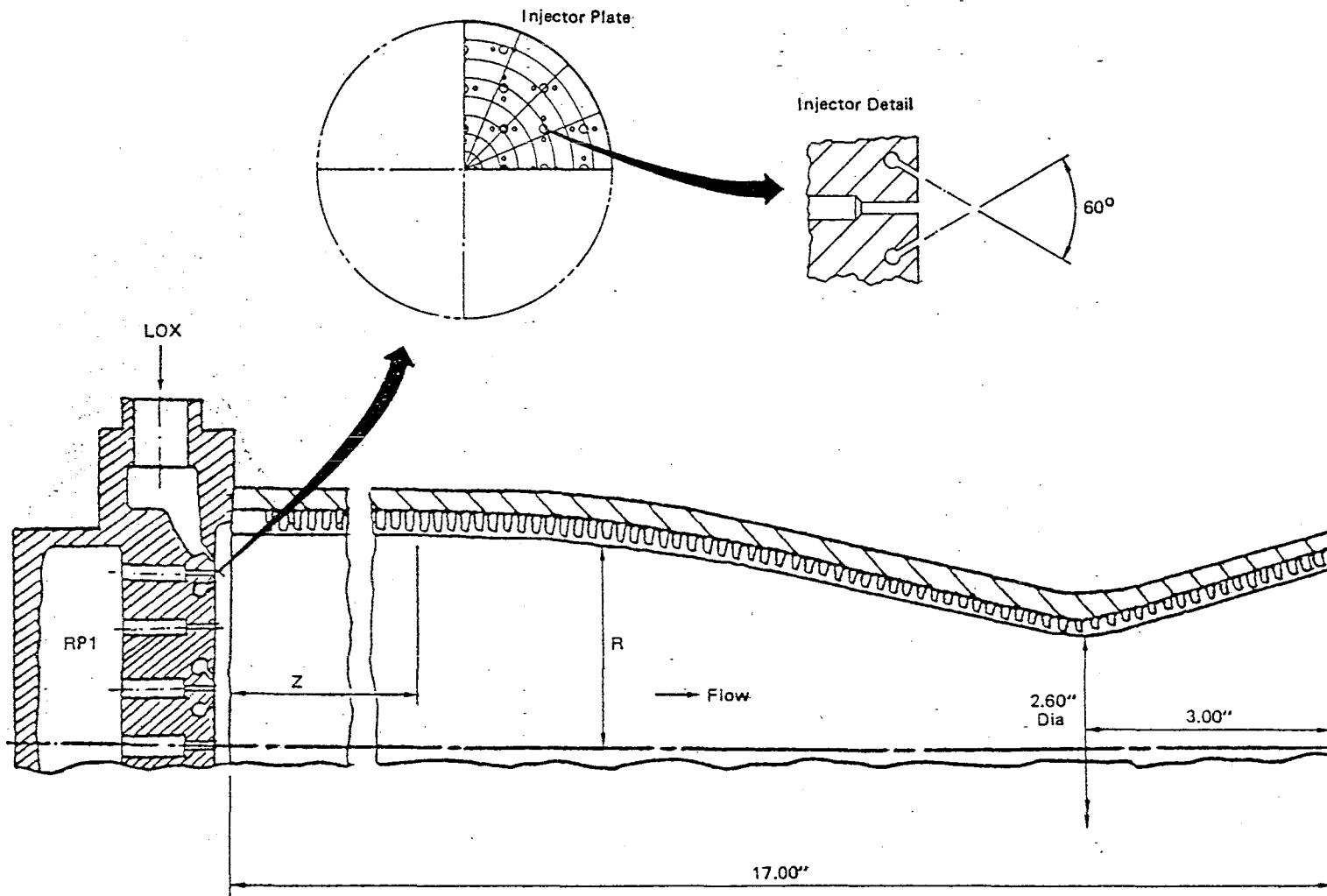
Figure 1.1 Rocket Engine Geometry and Injector Plate Configuration

The physical models in the care are: the k $\sim$ ϵ model of turbulence, one and two step finite-rate reaction models, and six-flux radiation model.

The numerical solution procedure employs a control-volume approach, with staggered grid and upwind-differencing practices. The solution scheme for Eulerian set of equations is a modified SIMPLE algorithm. These modifications include inproved equation solvers, under-relaxiation practices, and order of solving equations for different variables. For instance, velocities are solved by a point-by-point (Jacobi) method, while all other equations are solved simultaneously over the whole field.

The code has been checked for both numerical and physical considerations. Results of test calculations and parametric studies as well as recommendations for further improvements and verifications are presented in Volume II.

2.   INTRODUCTION

One of the significant ways in which the performance level of the rocket engines can be improved is by the use of optimal injector design, advanced materials and cooling concepts that allow a significant increase in thrust level. Figure 2.1 illustrates typical geometry of the rocket engine and selected injector element configurations. Injectors usually take the form of a perforated disk at the head of the rocket engine combustor and can vary in shape and dimension. Injection characteristics are improtant for proper mixing, evaporation, and efficient and stable combustion. The objective of the present project was to develop a predictive tool for rocket injection anomalies study.

In the past, the design of injectors has been primarily based on experimental tests, experience and intuition. More recently, injector design capability is being improved further by employing computer codes capable of predicting two-phase flow, evaporation, chemical reaction and heat transfer within the complex geometries of liquid fueled rocket einges. Performance characteristics of liquid oxygen/hydrocarbons (LOX/HC) propelled engines can be studied by simulating combustion processes for different propellant combinations, injector elements, cooling systems, and pressure levels.

A research program has been initiated by the National Aeronautics and Space Administration at the Lewis Research Center to provide a quantitatively accurate numerical modeling capability for the design and development of luqiid fueled rocket engines. The work has been performed at CHAM of North America Incorporated and resulted in a three-dimensional computer code (REFLAN3D-SPRAY) capable of predicting two-phase liquid fuel spray, combustion and heat transfer in engine combustors. An existing 3-D, CHAM computer code was modified to incorporate Eulerian-Lagrangean technique for two-phase spray simulation.

Full details of the adopted mathematical formulation, physical models, boundary conditions and solution procedures are described in this report. An accompanying report, Volume 2, describes the results of various numerical consistency test cases, and parametric studies as well as the recommendation for further improvements and verification of the code.
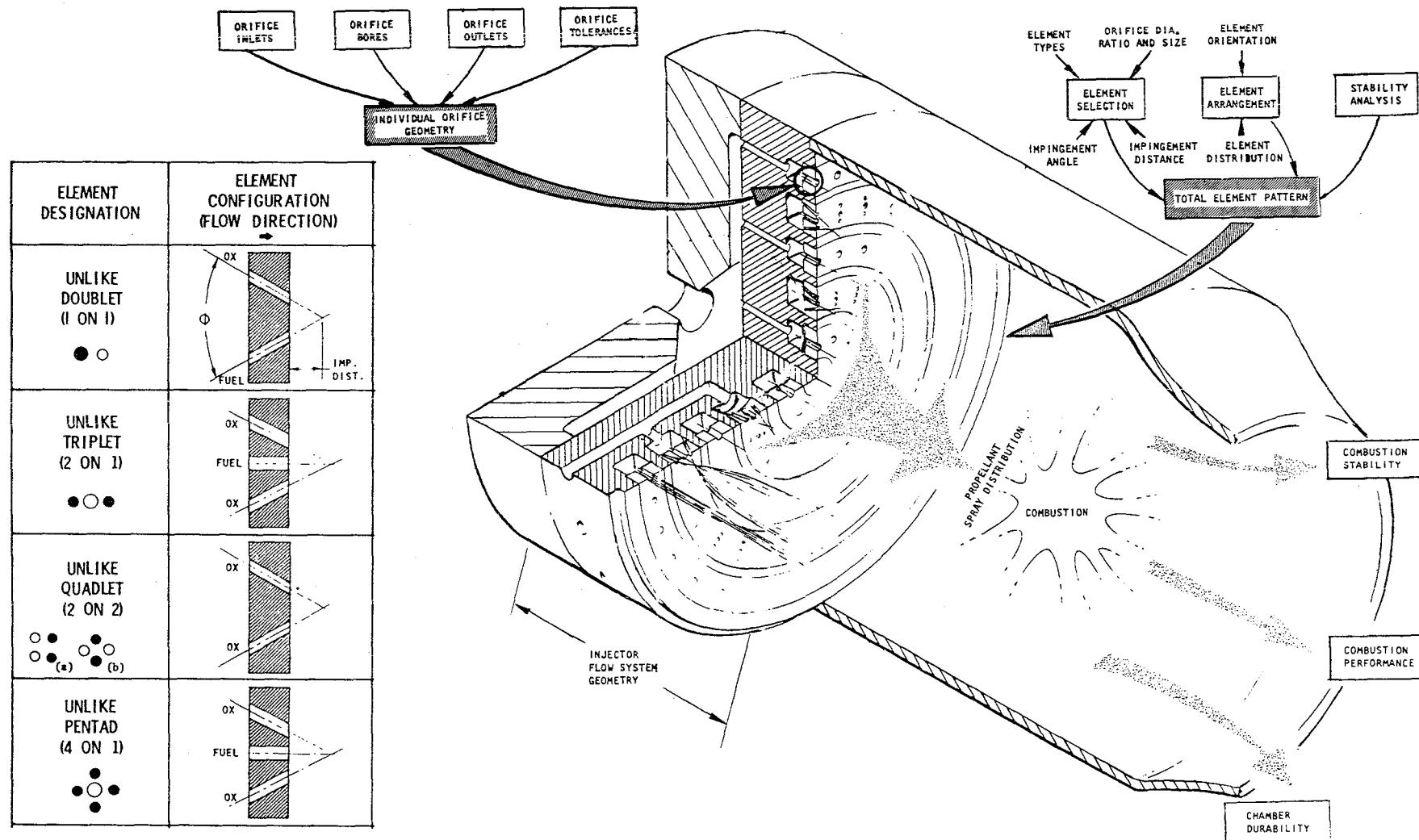
Figure 2.1 Liquid Fueled Rocket Engine and Typical Injector Configurations

3. MATHEMATICAL BASIS

3.1 Introduction

This chapter describes mathematical formulation of the two-phase flow, heat transfer and combustion phenomena handled by the REFLAN3D -SPRAY code. In the first section, basic principles of the Eulerian-Lagrangean (E-L) approach are presented. The second and third sections provide mathematical description of the physical processes in Eulerian and Lagrangean frames, respectively. The formulation is presented in fairly general terms so as to be applicable to the wide range of flow situations.

3.2 Eulerian-Lagrangean Approach

The mathematical formulation of the two-phase flow and combustion processes comprises the application of Eulerian conservation equations to the gas-phase and Lagrangean equations of droplet motion and thermal balance. The Eulerian part of the method involves solution of the following gas phase equations:

- continuity equation;
- three momentum equations;
- energy equation;
- turbulence kinetic energy and dissipation rate equations;
- unburned fuel and CO mass fraction equations;
- mixture fraction (composite fuel fraction) equation; and
- radiation equations.

The Lagrangean part is accomplished by integrating the droplet equations of:

- motion;
- heat transfer; and
- mass balance

along their trajectory.

The spray combustion model assumes that the evaporating droplets act as spacially distributed sources of fuel vapor. The link between the phases involves mass, momentum and energy coupling and is mathematically expressed in terms of interphase transfer source terms in all Eulerian equations.

The complete solution algorithm for a gas-droplet spray flow is presented in Figure 3.1.
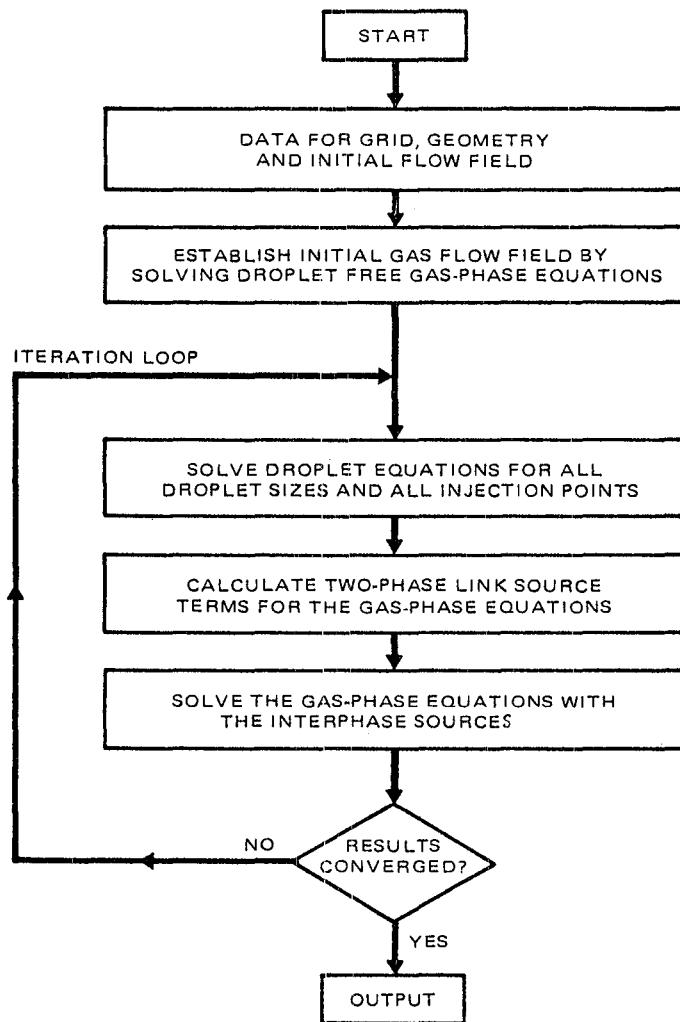
Figure 3.1 Flow Chart of the E-L Solution Algorithm

First grid and geometry data are specified and flow field variables are initialized. A droplet-free solution of the gas field is then obtained at the begining of the iteration cycle. This flow field is used for droplet trajectories, size and temperature calculations. The mass, momentum and energy interphase source terms are then determined. These source terms are now incorporated into the gas field equations. The new gas flow field solution is used again the the solution of the droplet equation. Thus there is a two-way coupling between the gas and liquid phase equations. The calculation porcess is continued until the converged solution is obtained.

3.3　Basic Eulerian Equations

3.3.1　Fluid Flow Equations

The hydrodynamic equations are expressed in three-dimensional, cylindrical polar coordinates x-r-θ, as follows:

Continuity

$$\frac{\partial \rho}{\partial t} + \frac{\partial}{\partial x}(\rho u) + \frac{1}{r}\frac{\partial(\rho v r)}{\partial r} + \frac{1}{r}\frac{\partial}{\partial \theta}(\rho w) = \dot{m}_{int} \qquad (3.3\text{-}1)*$$

x-Momentum

$$\frac{\partial}{\partial t}(\rho u) + \frac{\partial}{\partial x}(\rho u^2) + \frac{1}{r}\frac{\partial}{\partial r}(r\rho v u) + \frac{1}{r}\frac{\partial}{\partial \theta}(\rho w u) - \frac{\partial}{\partial x}\left(\mu\frac{\partial u}{\partial x}\right) - \frac{1}{r}\frac{\partial}{\partial r}\left(\frac{r\mu\partial u}{\partial r}\right) - \frac{1}{r}\frac{\partial}{\partial \theta}\left(\frac{\mu}{r}\frac{\partial u}{\partial \theta}\right)$$

$$= \frac{-\partial p}{\partial x} + \frac{\partial}{\partial x}\left(\mu\frac{\partial u}{\partial x}\right) + \frac{1}{r}\frac{\partial}{\partial r}\left(\mu r\frac{\partial v}{\partial x}\right) + \frac{1}{r}\frac{\partial}{\partial \theta}\left(\mu\frac{\partial w}{\partial x}\right) - \frac{2}{3}\frac{\partial}{\partial x}\left\{\mu\left(\frac{\partial u}{\partial x} + \frac{1}{r}\frac{\partial}{\partial r}(rv) + \frac{1}{r}\frac{\partial w}{\partial \theta}\right) + \rho k\right\}$$

$$+ S_{int}^{u} \qquad (3.3\text{-}2)**$$

r- Momentum

$$\frac{\partial(\rho v)}{\partial t} + \frac{\partial(\rho u v)}{\partial x} + \frac{1}{r}\frac{\partial}{\partial r}(r\rho v^2) + \frac{1}{r}\frac{\partial}{\partial \theta}(\rho v w) - \frac{\partial}{\partial x}\left(\mu\frac{\partial v}{\partial x}\right) - \frac{1}{r}\frac{\partial}{\partial r}\left(r\mu\frac{\partial v}{\partial r}\right) - \frac{1}{r}\frac{\partial}{\partial \theta}\left(\frac{\mu}{r}\frac{\partial v}{\partial \theta}\right)$$

$$= \frac{-\partial p}{\partial r} + \frac{\partial}{\partial x}\left(\mu\frac{\partial u}{\partial r}\right) + \frac{1}{r}\frac{\partial}{\partial r}\left(\mu r\frac{\partial v}{\partial r}\right) + \frac{1}{r}\frac{\partial}{\partial \theta}\left\{\mu\left(\frac{\partial w}{\partial r} - \frac{w}{r}\right)\right\} - \frac{2\mu}{r}\left(\frac{1}{r}\frac{\partial w}{\partial \theta} + \frac{v}{r}\right) + \rho w^2/r$$

$$\frac{-2}{3}\frac{\partial}{\partial r}\left\{\mu\left(\frac{\partial u}{\partial x} + \frac{1}{r}\frac{\partial}{\partial r}(rv) + \frac{1}{r}\frac{\partial w}{\partial \theta}\right) + \rho k\right\} + S_{int}^{v} \qquad (3.3\text{-}3)$$

---

* See Nomenclature for explanation of symbols.
**Note that for Cartesian coordinates, $r\to\infty$, $\partial r \equiv \partial y$ and $r\partial \equiv \partial z$.

θ-momentum

$$\frac{\partial \rho w}{\partial t} + \frac{\partial}{\partial x}(\rho u w) + \frac{1}{r}\frac{\partial}{\partial r}(r\rho v w) + \frac{1}{r}\frac{\partial}{\partial \theta}(\rho w^2) - \frac{\partial}{\partial x}\left(\frac{\mu \partial w}{\partial x}\right) - \frac{1}{r}\frac{\partial}{\partial r}\left(\frac{r\mu \partial w}{\partial r}\right) - \frac{1}{r}\frac{\partial}{\partial \theta}\left(\frac{\mu}{r}\frac{\partial w}{\partial \theta}\right)$$

$$= \frac{-1}{r}\frac{\partial p}{\partial \theta} + \frac{\partial}{\partial x}\left(\frac{\mu}{r}\frac{\partial u}{\partial \theta}\right) + \frac{1}{r}\frac{\partial}{\partial r}\left\{\mu r\left(\frac{1}{r}\frac{\partial v}{\partial \theta} - \frac{w}{r}\right)\right\} + \frac{1}{r}\frac{\partial}{\partial \theta}\left\{\frac{\mu}{r}\left(\frac{\partial w}{\partial \theta} + 2v\right)\right\} + \frac{\mu}{r}\left(\frac{\partial w}{\partial r} + \frac{1}{r}\frac{\partial v}{\partial \theta} - \frac{w}{r}\right)$$

$$- \frac{\rho v w}{r} - \frac{2}{3}\frac{1}{r}\frac{\partial}{\partial \theta}\left\{\mu\left(\frac{\partial u}{\partial x} + \frac{1}{r}\frac{\partial}{\partial r}(rv) + \frac{1}{r}\frac{\partial w}{\partial \theta}\right) + \rho k\right\} + S_{int}^W \tag{3.3-4}$$

In the above equations, u, v and w are velocity components in the x, r and θ directions, respectively; p is the pressure; ρ and μ are respectively the density and viscosity of the fluid mixture, which may be non-uniform. The normal-stress terms involving bulk viscosity (which is zero for most fluids including oxygen and RP1 fuel) have been omitted from the momentum equations.

By multiplying equation (3.3-4) by r, and rearranging, a new θ momentum equation can be obtained with angular velocity W ≡ rw as a dependent variable. Experience indicates that some of the shear stresses expressed in the new form are easier to handle during numerical claculations. The transformed form of the θ-momentum equation is:

θ-momentum

$$\frac{\partial \rho W}{\partial t} + \frac{\partial}{\partial x}(\rho u W) + \frac{1}{r}\frac{\partial}{\partial r}(\rho r v W) + \frac{1}{r}\frac{\partial}{\partial \theta}(\rho W^2) - \frac{\partial}{\partial x}\left(\mu \frac{\partial W}{\partial x}\right) - \frac{1}{r}\frac{\partial}{\partial r}\left(r\mu \frac{\partial W}{\partial r}\right) - \frac{1}{r}\frac{\partial}{\partial \theta}\left(\frac{\mu}{r}\frac{\partial W}{\partial \theta}\right)$$

$$= -\frac{1}{r}\frac{\partial p}{\partial \theta} + \frac{\partial}{\partial x}\left(\mu \frac{\partial u}{\partial \theta}\right) + \frac{\partial}{\partial r}\left(\mu \frac{\partial v}{\partial \theta}\right) + \frac{1}{r^2}\frac{\partial}{\partial \theta}\left(\mu \frac{\partial W}{\partial \theta}\right) + \frac{2}{R}\frac{\partial \mu v}{\partial \theta} + \frac{\mu}{r}\frac{\partial v}{\partial \theta} - \frac{2}{r}\frac{\partial \mu W}{\partial r}$$

$$- \frac{2}{3}\frac{1}{r}\frac{\partial}{\partial \theta}\left\{\mu\left(\frac{\partial u}{\partial x} + \frac{1}{r}\frac{\partial(rv)}{\partial v} + \frac{1}{r^2}\frac{\partial W}{\partial \theta}\right) + \rho k\right\} + S_{int}^W \tag{3.3-4a}$$

Equation 3.3-4a is used in the code. For laminar flows, the velocity components are the instantaneous ones; and μ is the molecular viscosity of the fluid mixture. For turbulent flows, it shall be assumed that the same equations are valid. For such situations, the time-mean values of all the flow variables and fluid properties are used, and μ is

now the effective viscosity(which is the molecular viscosity augmented by the turbulent contribution). These comments also apply to the other equations which shall be considered in the following sections.

Equations (3.3-1) to (3.3-4) govern the variation of the velocity components u, v, w, and the pressure p. In order to solve these equations, information about the variations of density ρ and viscosity μ is required. This is discussed next.

3.3.2 Density and Viscosity

The density is related to pressure, temperature and the composition of the gas mixture through an equation of state:

$$\rho = \rho\ (p,\ T,\ m_j) \tag{3.3-5}$$

where T is the temperature of the fluid mixture, and the m_j's are the mass fractions of the component species of the mixture. Variations of T and m_j's are obtained either from part of the problem specification, or from the solution of additional differential equations.

In REFLAN-3D, density is calculated from the following formula:

$$\rho = \frac{p\ \bar{M}}{R\ T} \tag{3.3-6}$$

where $\frac{1}{\bar{M}} = \Sigma\ \left(\frac{m}{M}\right)_j$ \hfill (3.3-7)

and where R is the gas constant and M_j is molecular weight. Summation is taken over all species.

For the evaluation of viscosity, laminar and turbulent flows have to be considered separately. For laminar flows, the viscosity is assumed to be a function of temperature and mixture composition:

$$\mu = \mu\ (T,\ m_j) \tag{3.3-8}$$

For turbulent flows, however, the problem is more complicated. The turbulent contribution (μ_t) to the effective viscosity is a function of local quantities such as velocity gradients, etc. The evaluation of μ_t and the turbulence

3-5

model are discussed in the next section.

3.4 The Turbulence Model

3.4.1 The $k{\sim}\varepsilon$ Model

The $k \sim \varepsilon$ model of turbulence is most commonly used for prediction of complex flow problems. The basis of the model is that it solves the transport equations for turbulence kinetic energy and turbulence dissipation rate.

The turbulence model incorporated into the REFLAN3D code is the high Reynolds number $k{\sim}\varepsilon$ two-equation model recommended by Launder and Spalding (Reference 1). In the following section the governing equations are presented. Details of the derivation can be found in the published literature (References 1, 2, 3) and are not provided in this report.

3.4.2 Governing Equations for the $k{\sim}\varepsilon$ Turbulence Model

The basic differential equations for the turbulence kinetic energy k, and its dissipation rate ε, are:

$$\frac{\partial}{\partial x}(\rho u k) + \frac{1}{r}\frac{\partial}{\partial r}(r\rho v k) + \frac{1}{r}\frac{\partial}{\partial \theta}(\rho w k) - \frac{\partial}{\partial x}\left(\Gamma_{k,eff}\frac{\partial k}{\partial x}\right) - \frac{1}{r}\frac{\partial}{\partial r}\left(r\Gamma_{k,eff}\frac{\partial k}{\partial r}\right)$$

$$- \frac{1}{r}\frac{\partial}{\partial \theta}\left(\Gamma_{k,eff}\frac{1}{r}\frac{\partial k}{\partial \theta}\right) = G_k - \rho\varepsilon \tag{3.4-1}$$

$$\frac{\partial}{\partial x}(\rho u \varepsilon) + \frac{1}{r}\frac{\partial}{\partial r}(r\rho v \varepsilon) + \frac{1}{r}\frac{\partial}{\partial \theta}(\rho w \varepsilon) - \frac{\partial}{\partial x}\left(\Gamma_{\varepsilon,eff}\frac{\partial \varepsilon}{\partial x}\right) - \frac{1}{r}\frac{\partial}{\partial r}\left(r\Gamma_{\varepsilon,eff}\frac{\partial \varepsilon}{\partial r}\right)$$

$$- \frac{1}{r}\frac{\partial}{\partial \theta}\left(\Gamma_{\varepsilon,eff}\frac{1}{r}\frac{\partial \varepsilon}{\partial \theta}\right) = (C_1 G_k - C_2\rho\varepsilon)\,\varepsilon/_k + \rho\varepsilon\nabla\vec{U} \tag{3.4-2}$$

In the above equations G_k is the generation term for the kinetic energy of turbulence and is given by:

$$G_k = \mu_t \{ 2\{ (\frac{\partial u}{\partial x})^2 + (\frac{\partial v}{\partial r})^2 + (\frac{1}{r}\frac{\partial w}{\partial \theta} + \frac{v}{r})^2 \} + (\frac{\partial w}{\partial x} + \frac{1}{r}\frac{\partial u}{\partial \theta})^2 + (\frac{\partial u}{\partial r} + \frac{\partial v}{\partial x})^2$$

$$+ (\frac{\partial w}{\partial r} + \frac{1}{r}\frac{\partial v}{\partial \theta} - \frac{w}{r})^2 \} \qquad\qquad (3.4\text{-}3)$$

The quantities C_D, C_1 and C_2 are constants, $\Gamma_{k,eff}$ and $\Gamma_{\varepsilon,eff}$ are the effective* exchange coefficients for k and ε, respectively, and are given by:

$$\Gamma_{k,eff} = \mu_{eff}/\sigma_{k,eff} \qquad\qquad (3.4\text{-}4)$$

$$\Gamma_{\varepsilon,eff} = \mu_{eff}/\sigma_{\varepsilon,eff} \qquad\qquad (3.4\text{-}5)$$

where $\sigma_{k,eff}$ and $\sigma_{\varepsilon,eff}$ are the effective Schmidt numbers for k and ε and are assumed to be constant.

3.4.3 Turbulent and Effective Viscosities

The turbulent viscosity μ_t is related to k and ε, via:

$$\mu_t = C_D \rho k^2/\varepsilon \qquad\qquad (3.4\text{-}6)$$

and, the effective viscosity is given by:

$$\mu_{eff} = \mu_t + \mu_\ell \qquad\qquad (3.4\text{-}7)$$

where μ_ℓ is the laminar or molecular viscosity of the fluid. Often μ_t is very large compared with μ_ℓ, and μ_{eff} can be taken equal to μ_t without introducing serious errors. The first practice (equation 3.4-7) is employed in the REFLAN3D code.

Recommended values (Reference 3) for the constants appearing in the above equations are:

$$C_D \quad = 0.09;$$

$$C_1 \quad = 1.43;$$

$$C_2 \quad = 1.92; \text{ and}$$

---

* The subscript "eff", to denote effective values, is used explicitly when coefficients that are related to turbulent flows exclusively are involved, otherwise non-subscripted symbols will be used.

$$\sigma_{k,eff} = 0.90. \tag{3.4-8}$$

The Schmidt numbers $\sigma_{\varepsilon,eff}$ for the dissipation rate of turbulence is calculated from:

$$\sigma_{\varepsilon,eff} = \frac{\kappa^2}{(C_2 - C_1)\, C_D^{\;1/2}} \tag{3.4-9}$$

where κ is the Von Karman constant. A value of 0.4 is assumed for κ.

3.5 The Energy Balance Equation

3.5.1 The Stagnation Enthalpy Equation

The stagnation enthalpy $\tilde{h}$, defined as:

$$\tilde{h} \equiv C_p T + \Sigma m_j H_j + \frac{1}{2}(u^2 + v^2 + w^2) \quad , \tag{3.5-1}$$

is a dependent variable in the energy transport equation:

$$\frac{\partial}{\partial x}(\rho u \tilde{h}) + \frac{1}{r}\frac{\partial}{\partial r}(r \rho v \tilde{h}) + \frac{1}{r}\frac{\partial}{\partial \theta}(\rho w \tilde{h}) - \frac{\partial}{\partial x}\left(\Gamma_{\tilde{h}} \frac{\partial \tilde{h}}{\partial x}\right) - \frac{1}{r}\frac{\partial}{\partial r}\left(r \Gamma_{\tilde{h}} \frac{\partial \tilde{h}}{\partial r}\right)$$

$$- \frac{1}{r}\frac{\partial}{\partial \theta}\left(\Gamma_{\tilde{h}} \frac{1}{r}\frac{\partial \tilde{h}}{\partial \theta}\right) = S_{\tilde{h}} + S_{int}^{\tilde{h}} \quad . \tag{3.5-2}$$

In the above equations, C_p is the mixture specific heat, H_j is the heat of combustion of the j-th species, $S_{\tilde{h}}$ represents the sum of all gas-phase source terms including thermal radiation (discussed below) and $S_{int}^{\tilde{h}}$ represents interphase energy transfer source term.

Equation (3.5-2) has been obtained with the assumption that the exchange coefficients for the transport of the mixture and for heat conduction are all equal at a point, although they may vary from point to point.

It should be remarked that under certain circumstances the variation of the specific enthalpy $\tilde{h}$ can be obtained without solving the differential equation (3.5-2). For example, consider the incompressible flow of initially unmixed reactants in an enclosure with adiabatic, impermeable, non-catalytic walls and without any thermal radiation. A non-dimensional enthalpy ϕ_h can be

defined as:

$$\phi_h \equiv \frac{\tilde{h} - \tilde{h}_A}{\tilde{h}_F - \tilde{h}_A} \tag{3.5-3}$$

where the subscripts F and A refer to the inlet fuel and oxidant streams, respectively. The differential equation for the variable ϕ_h is then identical to that for the mixture fraction f in every respect, including the boundary conditions. Thus, $\tilde{h}$ and f are linearly related. If the reactants are pre-mixed and uniform in composition, then the enthalpy must be uniform throughout.

Once the enthalpy and the species concentrations have been determined, the temperature T can be determined from equation (3.5-1) viz:

$$T = \frac{\tilde{h} - \Sigma m_j H_j - \frac{1}{2}(u^2 + v^2 + w^2)}{C_p} \tag{3.5-4}$$

The specific heat C_p, however, is a function of temperature and the composition:

$$C_p = \sum_j m_j (a_j + b_j T + c_j T^2 + d_j T^3 + e_j T^4) \tag{3.5-5}$$

where aj, bj, cj, dj and ej are constants for each chemical specie.

The $C_p \sim T$ dependence is weak so the system (3.5-4) and (3.5-5) does not require iterations. Usually the previous iteration value for T is used to calculate C_p and then (3.5-4) is used to calculate new temperature.

3.6   Thermal Radiation

3.6.1 Introduction

There exist few numerical procedures for handling the radiation integro-differential equations. Of these the "zone method" of Hottel (Reference 4) and "Monte Carlo method" (Reference 5) are well known and tested. Recently introduced "beam tracing method" (Reference 6) at this stage of development is not suitable for engineering applications. All three procedures require significant quantities of computer time and/or storage.

The iterative nature of reactive flow calculations requires simple and fast algorithms for radiation calculations. The most commonly used method for radiation simulation is the "flux model" originated by Schuster (Reference 7) and Hamaker (Reference 8) in astrophysics. Flux methods are based on the

use of some simplifying assumptions for the angular variation of the radiation intensity. This allows the exact integro-differential radiation transport equation to be reduced to a system of approximate differential equations in the space variable only. These are ideally suited to numerical solutions simultaneously with the flow equations.

The six-flux method is described below for three-dimensional flow calculations.

3.6.2 The Six-Flux Method

For an absorbing-emitting grey medium in local thermodynamic equilibrium the radiation transport equation can be written as (Reference 9):

$$\vec{\Omega} \cdot \nabla I_r = -aI_r + a\frac{E}{\pi} + \frac{s}{4\pi} \int_{4\pi} I d\Omega \tag{3.6-1}$$

where I is the radiation intensity, $\vec{\Omega}$ is a unit vector representing direction of radiating beam, a is absorption, s is a scattering coefficient, $E = \sigma \cdot T^4$, and σ is the Bolzman constant. Central to the assumption of a flux model is the assumed variation of the intensity with direction. Assumption of constant I in a quadrant centered along each ($\pm$) coordinate direction results in six differential equations for intensities (Reference 10).

$$\frac{d}{dr}(rI) = r\{-(a+s)I + \frac{J}{r} + aE + \frac{s}{6}(I + J + K + L + M + N)\}$$

$$\frac{d}{dr}(rJ) = r\{(a+s)I + \frac{J}{r} + aE - \frac{s}{6}(I + J + K + L + M + N)\}$$

$$\frac{dK}{dX} = -(a+s)K + aE + \frac{s}{6}(I + J + K + L + M + N)$$

$$\frac{dL}{dX} = (a+s)L - aE - \frac{s}{6}(I + J + K + L + M + N) \tag{3.6-2}$$

$$\frac{1}{r}\frac{dM}{d\theta} = -(a+s)M + aE + \frac{s}{6}(I + J + K + L + M + N)$$

$$\frac{1}{r}\frac{dN}{d\theta} = (a+s)N - aE - \frac{s}{6}(I + J + K + L + M + N)$$

The I, J, K, L, M and N are the radiation fluxes in y^+, y^-, x^+, x^-, θ^+, θ^- directions, respectively.

The net radiation heat fluxes, used in the energy equation source term can be evaluated from:

$$Q_y = I - J = - \frac{2}{a + s + 1/r} \cdot \frac{d(I + J)}{dr}$$

$$Q_x = K - L = - \frac{2}{a + s} \frac{d(K + L)}{dx} \tag{3.6-3}$$

$$Q_\theta = M - N = - \frac{2}{a + s} \frac{1}{r} \frac{d(M + N)}{d\theta}$$

It can be seen that only composite fluxes $(I + J)$, etc. are used for the heat flux calculation. It is convenient, therefore, to add appropriate equations of the system (3.6-2) and arrive at the working equations for the "composite fluxes" R_x, R_y and R_z viz:

$$\frac{d}{dx} \left(\frac{1}{a+s} \frac{dR_x}{dx} \right) = - \{ a (R_x - E) + \frac{S}{3} (2 R_x - R_y - R_z) \}$$

$$\frac{d}{dr} \left(\frac{r}{a+s+\frac{1}{r}} \frac{dR_y}{dr} \right) = - r \{ a (R_y - E) + \frac{S}{3} (2R_y - R_x - R_z) \} \tag{3.6-4}$$

$$\frac{1}{r} \frac{\partial}{\partial\theta} \left(\frac{1}{a+s} \frac{1}{r} \frac{dR_z}{d\theta} \right) = - \{ a (R_z - E) + \frac{S}{3} (2R_z - R_x - R_y) \}$$

where:

$$R_x \equiv \frac{1}{2} (I + J)$$

$$R_y \equiv \frac{1}{2} (K + L) \tag{3.6-5}$$

$$R_z \equiv \frac{1}{2} (M + N)$$

The composite radiation-flux equations are easy to solve second order (diffusive type) ODE. They are coupled with the stagnation enthalpy equation through the presence of R_x, R_y and R_z in the source term of the latter. Indirect coupling to other equations also occurs through the temperature appearing in the emissive power E and through any dependence of the coefficients a and s on the local quantities m_{fu}, m_{CO_2}, m_{H_2O}, etc.

The contribution of the radiation fluxes to the stagnation-enthalpy source term is given by:

$$(S_h) _{radiation} = 2a \{ (R_y - E) + (R_x - E) + (R_z - E) \} \tag{3.6-6}$$

Since information on the variations of the coefficients a and s with other quantities is often scarce and imprecise, they have simply been assumed to be constant in REFLAN3D. However, should knowledge of the variations be available, it is not a major problem to incorporate these into the code. It may be noted that when the absorption coefficient a is very large, R_x, R_y and R_z become very nearly equal to the direct emission E.

3.7 Chemistry Equations

3.7.1 Reaction Models

There are three levels of complexity for simulating the chemical kinetics in the REFLAN3D code:

- instantaneous reaction assumption;
- one step reaction mechanism; and
- two step mechanism with intermediate CO.

The rate of chemical reaction is assumed to be governed by an Arrhenius expression for laminar flows, and by the "Eddy-Break-Up" model (Reference 11) for turbulent flows.

Details of the combustion models and the chemistry equations are described below.

3.7.2 Conservation Equation for a Chemical Species j

The conservation equation for a chemical species j is:

$$\frac{\partial}{\partial x}(\rho u m_j) + \frac{1}{r}\frac{\partial}{\partial r}(r\rho v m_j) + \frac{1}{r}\frac{\partial}{\partial \theta}(\rho w m_j) - \frac{\partial}{\partial x}(\Gamma_j \frac{\partial m}{\partial x} j)$$

$$- \frac{1}{r}\frac{\partial}{\partial r}(r\Gamma_j \frac{\partial m}{\partial r} j) - \frac{1}{r}\frac{\partial}{\partial \theta}(\Gamma_j \frac{1}{r}\frac{\partial m}{\partial \theta} j) = R_j \qquad (3.7-1)$$

where m_j is the mass fraction of chemical species j; R_j is the mass rate of creation of species j by chemical reaction, per unit volume; and Γ_j is the exchange coefficient. For a chemically-inert species R_j is, by definition, zero.

3.7.3 Mixture Fraction and Inert Species Equations

The simple single-step reaction of a pair of reactants (called here for convenience fuel (fu) and oxidant (ox)) can be expressed in the following stoichiometric relation:

$$1 \text{ kg fu} + s \text{ kg ox} \rightarrow (1 + s) \text{ kg products} \tag{3.7-2}$$
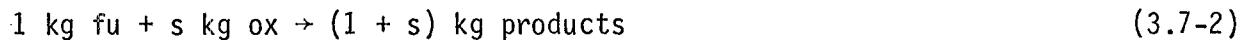
where s represents the stoichiometric oxidant/fuel ratio and is a constant for a given reactant pair. It should be noted that the reaction equation (3.7-2) does not impose any restrictions on the constitution of the reactants; thus the reactants may be mixtures, e.g. fuel $\equiv CO + H_2 + N_2$, oxidant $\equiv O_2 + N_2$.

An important consequence of the simple chemical reaction assumption is that the mass rates of creation by chemical reaction of fuel, oxidant, and product, R_{fu}, R_{ox} and R_{pr}, are related through:

$$R_{fu} = R_{ox}/s = -R_{pr}/(1 + s) \tag{3.7-3}$$

These relations can be made use of to yield conservation equations that have zero source terms.

It is further supposed that the exchange coefficients of fuel and oxidant are equal at each point in the flow, although they may still vary from point to point. It follows that equation (3.7-1) for oxygen (j≡ox) can be divided by s and subtracted from the corresponding equation for fuel (j≡fu).

The result is:

$$\frac{\partial}{\partial x}(\rho u \gamma) + \frac{1}{r}\frac{\partial}{\partial r}(r\rho v \gamma) + \frac{1}{r}\frac{\partial}{\partial \theta}(\rho w \gamma) - \frac{\partial}{\partial x}\frac{(\Gamma \partial \gamma)}{\partial x} - \frac{1}{r}\frac{\partial}{\partial r}(r\Gamma\frac{\partial \gamma}{\partial r}) - \frac{1}{r}\frac{\partial}{\partial \theta}(\Gamma\frac{1}{r}\frac{\partial \gamma}{\partial \theta}) = 0.$$

$$\tag{3.7-4}$$

where $\gamma \equiv m_{fu} - m_{ox}/s$ $\hspace{2cm}$ (3.7-5)

This is an equation having a single dependent variable, namely γ, and no source term; the two reaction-rate terms have cancelled out. To make equation (3.7-4) more general, a normalized dependent variable f ("mixture fraction") defined as:

$$f \equiv \frac{\gamma - \gamma_A}{\gamma_F - \gamma_A} \; ; \; 0 \leq \gamma < 1 \qquad\qquad (3.7\text{-}6)$$

can be introduced. The F and A indices represent conditions at fuel and air entry, respectively (Figure 3.7-1).
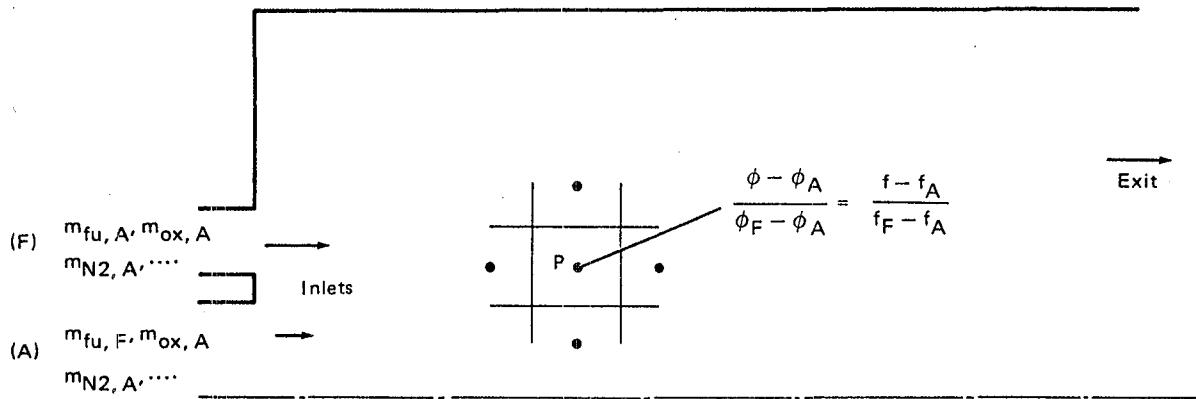
Figure 3.7-1 Specification of Inlet Composition at F- and A-inlets

The mixture fraction transport equation is written as:

$$\frac{\partial}{\partial x}(\rho u f) + \frac{1}{r}\frac{\partial}{\partial r}(r\rho v f) + \frac{1}{r}\frac{\partial(\rho w f)}{\partial \theta} - \frac{\partial}{\partial x}\left(\Gamma_f \frac{\partial f}{\partial x}\right) - \frac{1}{r}\frac{\partial}{\partial r}\left(r\Gamma_f \frac{\partial f}{\partial r}\right)$$

$$- \frac{1}{r}\frac{\partial}{\partial \theta}\left(\Gamma_f \frac{1}{r}\frac{\partial f}{\partial \theta}\right) = 0 \qquad\qquad (3.7\text{-}7)$$

The physical significance of the mixture fraction is that it represents the mass fraction of fuel in any form, i.e. fuel that has reacted and that has not. Thus, for chemically-inert flows, the mixture fraction f and the mass fraction of unburnt fuel m_{fu} would be identical.

Note that all atomic elements H, O, C, N (inert species) are governed by the source free transport equation identical to that of mixture fraction (3.7-8). For the equal exchange coefficient, zero source terms and linearly related boundary values,all inert species concentrations at any location are linearly related to f. Stoichiometric relations provide the auxiliary linear relations.

3.7.4 Stoichiometric Relations

The linear relation between the inert species ϕ and the mixture fraction f can be expressed as:

$$\frac{\phi - \phi_A}{\phi_F - \phi_A} = \frac{f - f_A}{f_F - f_A} \qquad (3.7-8)$$

where ϕ stands for m_C, m_O, m_H, m_N, etc., A and F indices represent A and F inlet, respectively.

For simple one-step reaction there are five species participating in the mixture composition viz: (fu, O_2, N_2, CO_2, H_2O). If two differential equations (f and m_{fu}) are solved, four additional algebraic equations can be obtained from relation (3.7-8).

If the A-jet composition consists only of air ($a_{ox} m_{ox} + (1-a_{ox}) m_{N2}$) and F-jet of fuel ($C_n H_m$) and say water vapor ($m_{fu,F}$, $m_{H_2O,F}$) the linear relations for atomic elements are:

$$m_C = 12 \cdot n' \, f \qquad (3.7-9)$$

$$m_H = (\frac{2}{18} m_{H_2O_F} + m'f_F) \frac{f}{f_F} \qquad (3.7-10)$$

$$m_O = a_{ox} - (a_{ox} - \frac{16}{18} m_{H_2O_F}) \frac{f}{f_F} \qquad (3.7-11)$$

On the other hand, stoichiometric relations can be written as:

$$m_C = 12 \, n' \, m_{fu} + \frac{12}{44} m_{CO_2} \qquad (3.7-12)$$

$$m_H = m' \, m_{fu} + \frac{2}{18} m_{H_2O} \qquad (3.7-13)$$

$$m_O = m_{ox} \quad \frac{16}{18} m_{H_2O} + \frac{32}{44} m_{CO_2} \qquad (3.7-14)$$

where $n' \equiv \frac{n}{12n + m}$ and $m' \equiv \frac{m}{12n + m}$

Combining equation (3.7-9) and (3.7-12) m_{CO_2} can be calculated. From equations (3.7-10) and (3.7-13) m_{H_2O} and from (3.7-10) and (3.7-14) m_{ox} can be determined.

$$m_{H_2O} = f \left(9\ m' + \frac{m_{H_2O_F}}{f_F}\right) - 9\ m'\ m_{fu} \qquad (3.7\text{-}15)$$

$$m_{CO_2} = 44\ n'f - 44\ n'\ m_{fu} \qquad (3.7\text{-}16)$$

$$m_{O_2} = a - f \left(\frac{a_{OX}}{f_F} + 32\ n' + 8\ m'\right) + m_{fu} \cdot (32\ n' + 8\ m') \qquad (3.7\text{-}17)$$

More complex formulae can be derived for arbitrary A-inlet and F-inlet composition.

Finally, since all the species mass fractions must add up to unity:

$$m_{fu} + m_{ox} + m_{CO_2} + m_{H_2O} + m_{N_2} = 1 \qquad (3.7\text{-}18)$$

Thus m_{N_2} can be obtained.

The technique of relating mixture composition to the mixture fraction f can be expressed on two examples of combustion regimes:

- diffusion controlled (instantaneous combustion); and
- kinetically influenced reactions.

These are described in the following sections.

3.7.5 Equations for Diffusion-Controlled Reactions

Before any reaction can take place, fuel and oxidant must be brought into physical contact with each other. It is thus expected that the reactant process is affected by both the rate at which mixing of the two reactants takes place and the rate of the chemical reaction itself. In situations where the fuel and oxidant are not initially mixed, the mixing rate, being in general much slower than the reaction rate, even in turbulent flows, controls the reaction process.   This leads to the assumption that thermodynamic equilibrium prevails everywhere. Thus, wherever fuel and oxidant are in contact, reaction will take place until one or the other has been completely consumed. Since chemical kinetics need not be considered under these circumstances, the complete chemical state can be determined by solving only one source-free conservation equation for the mixture fraction.

Once the f-equation (3.7-7) has been solved, the mass fractions of the other species can be obtained from algebraic equations.

The mass fractions of fuel and oxygen are related to the mixture fraction according to:

$$0 < f \leq f_{st} : \quad m_{fu} = 0$$

$$m_{ox} = (1 - f/f_{st}) \, m_{ox,inlet} \qquad (3.7\text{-}19)$$

$$1 > f \geq f_{st} : \quad m_{fu} = (f - f/f_{st})/(1 - f_{st})$$

$$m_{ox} = 0 \qquad (3.7\text{-}20)$$

In the above equations, f_{st} is the stoichiometric value of the mixture fraction and is given by:

$$f_{st} \equiv 1 / \left\{ 1 + s \left(\frac{m_{fu}}{m_{ox}}\right)_{inlet} \right\} \qquad (3.7\text{-}21)$$

The above equation is readily obtained from equation (3.7-6), noting that for stoichiometric mixtures, $m_{fu} \equiv m_{ox}/s$, and consequently $\gamma \equiv 0$. The physical significance of f_{st} is that the locus of all points where f has the value f_{st} defines the maximum reaction contour and hence the "flame envelope".

The linear relationships between the mixture fraction and the various mass fractions can be used to calculate m_{CO_2}, m_{H_2O}, etc. It should be remarked that these relationships are, strictly speaking, valid only for instantaneous values. Thus, for turbulent flows, where only the time-average values of the mixture fractions are available, the relationships of Figure 3.7-2 can be used only for time-average mass fractions. This is assumed in REFLAN3D code.

Some inaccuracy is involved in this assumption; it can be removed to some extent by, for example, solving an additional differential equation for the mean-square fluctuations of f (References 12, 13).

3-17
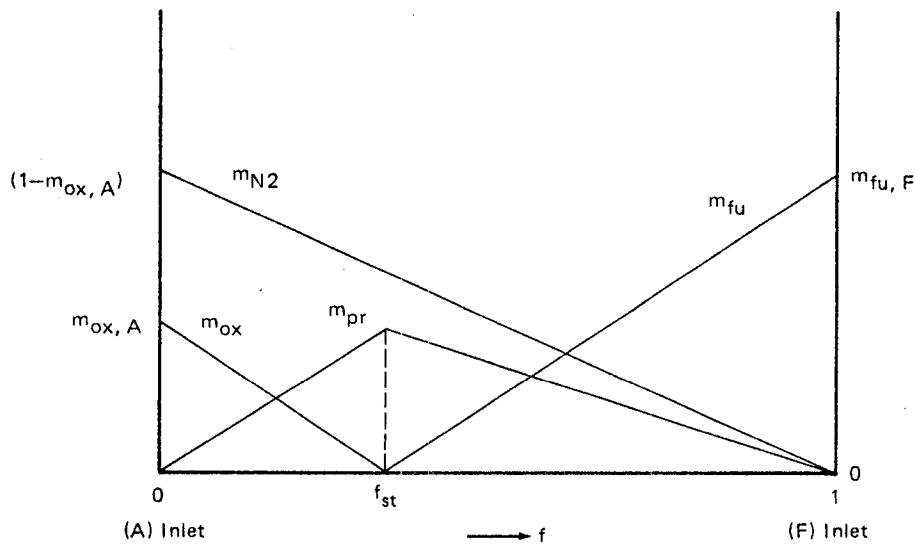
Figure 3.7-2. Diagram Showing the Variation of Mass Friction with f for a
Diffusion-Controlled Reaction

3.7.6 Equations for Kinetically-Influenced Reactions

When the chemical process is not physically controlled (as, for example, in the case of premixed fuel and oxidant mixtures) the rate of the chemical reaction will be the influencing factor. Since the assumption of thermodynamic equilibrium can no longer be used, solution of a source-free equation alone is not sufficient to determine all the species mass fractions. In addition, a conservation equation for one of the species must be solved. This could be any one of the three: m_{fu}, m_{ox}, or m_{pr}.

In REFLAN3D, for one-step reaction, two differential equations are solved: that for f, equation (3.7-7), and that for m_{fu}, equation (3.7-1) with j $\equiv$ fu. Under some circumstances, the solution of the f-equation may not be necessary even though the reaction is kinetically-controlled. For example, when a fuel-oxidant mixture of uniform composition is admitted into a chamber of impermeable, non-catalytic walls, under steady-state conditions, the source-free equation has the trivial solution: f is uniform everywhere and equal to the inlet value.

Once the mixture fraction f and the fuel mass fraction m_{fu} have been determined, the mass fraction of O_2, CO_2, H_2O and N_2 can be obtained from stoichiometric relations.

The variation of the species mass fractions with f for a kinetically-influenced reaction is shown in Figure 3.7-3.
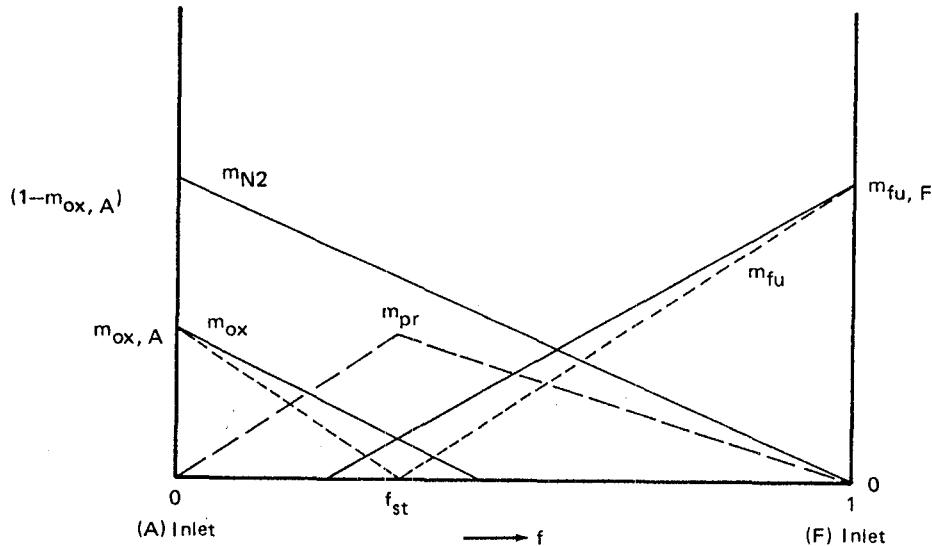
Figure 3.7-3. Diagram Showing the Variation of Mass Fractions with f for a Kinetically Influenced Reaction

NOTE: The dotted lines show the variations for a diffusion controlled reaction (as in Figure 3.7-2); the variation of m_{N_2} is the same for both.

3.7.7 Two-Step Reaction Model

A general hydrocarbon (C_nH_m) fuel oxidation is employed in two-step parametric reaction scheme as follows:

$$C_nH_m + (\lambda \frac{m + 2n}{4} + (1 - \lambda) \frac{m + 4n}{4}) O_2 \rightarrow \lambda n\ CO + (1 - \lambda)\ n\ CO_2 + \frac{m}{2} H_2O$$

$$\lambda n\ CO + \frac{\lambda n}{2} O_2 \qquad\qquad\qquad \rightarrow \lambda n\ CO_2 \qquad\qquad (3.7-22)$$
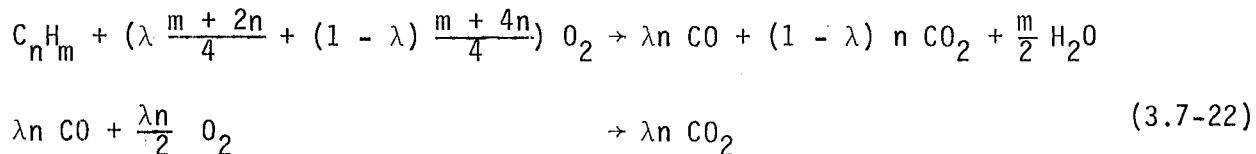
where m and n represent C_nH_m-hydrocarbon composition (e.g. for C_3H_8 n=3, m=8), and λ is the reaction scheme parameter (λ=0 for single step chemical reaction, and λ=1 for two step chemical reaction).

For certain cases (e.g. for heavy liquid hydrocarbons) $0<\lambda<1$ can represent simultaneous homogeneous-heterogeneous reactions at the droplet boundary layer.

3-19

There are six species (C_nH_m, CO_2, CO, H_2O and N_2) involved in the above reactions which have to be determined at each control cell of the combustion chamber.

Three properties viz: mixture fraction f, defined as a "total fuel" (burned or unburned), mass fraction of unburned fuel $m_{C_nH_m}$, and mass fraction of carbon monoxide m_{CO} are obtained from the differential equations. Three additional equations are obtained from the stoichiometric relations:

$$m_C = 12\ n'\ m_{C_nH_m} + \frac{12}{28}\ m_{CO} + \frac{12}{44}\ m_{CO_2}$$

$$m_H = m'\ m_{C_nH_m} + \frac{2}{18}\ m_{H_2O} \tag{3.7-23}$$

$$m_O = m_{O_2} + \frac{16}{28}\ m_{CO} + \frac{16}{18}\ m_{H_2O} + \frac{32}{44}\ m_{CO_2}$$

where $n' \equiv \dfrac{n}{12n + m}$ and $m' \equiv \dfrac{m}{12n + m}$

3.7.7 Reaction Rate Expressions

Two different options are considered for the reaction rate expression:

- Arrhenius expression; and
- Eddy-Break-Up model (EBU).

The Arrhenius expression for the bi-molecular reactions can be written as:

$$R_{fu,L} = -\rho A M_{FU} \left(\frac{\rho\ m_{FU}}{M_{FU}}\right)^\alpha \left(\frac{\rho\ m_{ox}}{M_{OX}}\right)^\beta \exp\ (-E/RT) \tag{3.7-24}$$

where A is reaction rate constant, E is the activation energy, R is the gas constant, M_{FU}, M_{OX} are molecular weights and α and β are reaction order constants. Similar expression holds for m_{CO} combustion rate.

For turbulent flows, apart from the usual need to use time-averaged quantities and effective transport coefficients, the effect of turbulence on the reaction rate should be separately accounted for. The eddy-Break-Up model of Spalding (Reference 11) assumes that the gas is composed of alternating fragments of unburned fuel and almost fully burned gas (premixed flame). The chemical reaction is supposed to occur on the interfaces between these two inkds of gragments.

The rate of reaction is supposed to depend upon the rate at which the fragments of unburnt gas are broken into still smaller fragments by the action of

turbulence, and is taken to be proportional to the rate of decay of turbulence energy. Thus, the rate of reaction is:

$$R_{fu,EBU} = - C_R \, \rho g^{\frac{1}{2}} \, \varepsilon/k \tag{3.7-25}$$

where C_R is a constant, and g represents the local mean-square concentration fluctuations.

The concentration fluctuation g can be determined by solving an additional equation having a form similar to that for the turbulence quantities $k \sim \varepsilon$ (References 12, 13). Magnussen (Reference 14) proposed an algebraic expression for g in the form:

$$g^{1/2} = \min \left(m_{fu}, \; \frac{m_{ox}}{s}, \; \frac{B \, m_{pr}}{1 + s} \right) \tag{3.7-26}$$

where $B = 4.5$ is an empirical constant.

For turbulent flows, the lower of the two reaction rates is often taken.

3.8   General Form of the Governing Differential Equations

All the differential equations discussed in the preceding sections are elliptic in nature and can be conveniently presented in the general form:

$$\frac{\partial}{\partial x} (\beta u \phi) + \frac{1}{r} \frac{\partial}{\partial r} (r \beta v \phi) + \frac{1}{r} \frac{\partial}{\partial \theta} (\beta w \phi) - \frac{\partial}{\partial x} \left(\Gamma_\phi \frac{\partial \phi}{\partial x} \right) - \frac{1}{r} \frac{\partial}{\partial r} \left(r \Gamma_\phi \frac{\partial \phi}{\partial r} \right)$$

$$- \frac{1}{r} \frac{\partial}{\partial \theta} \left(\Gamma_\phi \frac{1}{r} \frac{\partial \phi}{\partial \theta} \right) = S_\phi \tag{3.8-1}*$$

---

* 1. As a reminder, note that for Cartesian coordinates: $r \to \infty$, $\partial r \equiv \partial y$, and $r \partial \theta \equiv \partial z$.

  2. The differential equations for the three composite radiation-fluxes are of one-dimensional form. Thus the r- and θ-derivatives of this equation are absent for R_x, the x- and θ-derivatives are absent for R_y, and the x- and r-derivatives are absent for R_z.

Table 3.8-1. Summary of Equations for Three-Dimensional Flows

EQUATION	ϕ	β_ϕ	Γ_ϕ	S_ϕ	$S_{d\phi}$
continuity	1	ρ	0	0	$\dot{m}_{do} - m_{dI}$
axial x-momentum	u	ρ	μ	$-\dfrac{\partial p}{\partial x} + \dfrac{\partial}{\partial x}\left(\mu \dfrac{\partial u}{\partial x}\right) + \dfrac{1}{r}\dfrac{\partial}{\partial r}\left(r\mu \dfrac{\partial v}{\partial x}\right)$ $+ \dfrac{1}{r^2}\dfrac{\partial}{\partial \theta}\left(\mu \dfrac{\partial rw}{\partial x}\right) - \rho g_x +$ $- \dfrac{2}{3}\dfrac{\partial}{\partial x}\left(\mu_{eff}\,\nabla \cdot U + \rho k\right)$	$\dot{m}_d\left(u_{do} - u_{dI}\right)$
radial y-momentum	v	ρ	μ	$-\dfrac{\partial p}{\partial r} + \dfrac{\partial}{\partial x}\left(\mu \dfrac{\partial u}{\partial r}\right) + \dfrac{1}{r}\dfrac{\partial}{\partial r}\left(r\mu \dfrac{\partial v}{\partial r}\right)$ $+ \dfrac{1}{r}\dfrac{\partial}{\partial \theta}\left(\dfrac{\mu}{r} \dfrac{\partial rw}{\partial r}\right) - \dfrac{2}{r^3}\dfrac{\partial \mu rw}{\partial \theta} - \dfrac{2\mu}{r^3}\dfrac{\partial rw}{\partial \theta}$ $+ \dfrac{\rho w^2}{r} - \dfrac{2\mu}{r^2} v - \rho g_y$ $- \dfrac{2}{3}\dfrac{\partial}{\partial r}\left(\mu_{eff}\,\nabla \cdot U + \rho k\right)$	$\dot{m}_d\left(v_{do} - v_{dI}\right)$
circum-ferential θ-momentum	rw	ρ	μ	$-\dfrac{\partial p}{\partial \theta} + \dfrac{\partial}{\partial x}\left(\mu \dfrac{\partial u}{\partial \theta}\right) + \dfrac{\partial}{\partial r}\left(\mu \dfrac{\partial v}{\partial \theta}\right)$ $+ \dfrac{1}{r^2}\dfrac{\partial}{\partial \theta}\left(\mu \dfrac{\partial rw}{\partial \theta}\right) + \dfrac{2}{r}\dfrac{\partial \mu v}{\partial \theta} + \dfrac{\mu}{r}\dfrac{\partial v}{\partial \theta}$ $- \dfrac{2}{r}\dfrac{\partial \mu rw}{\partial r}$ $- \dfrac{2}{3}\cdot\dfrac{1}{r}\dfrac{\partial}{\partial \theta}\left(\mu_{eff}\,\nabla \cdot U + \rho k\right)$	$\dot{m}_d\left(rw_{do} - rw_{dI}\right)$
turbulence energy k	k	ρ	$\dfrac{\mu_{eff}}{\sigma_{k,eff}}$	$G_k - \rho\varepsilon$	$-\dot{m}_d k$

3-22

EQUATION	ϕ	β_ϕ	Γ_ϕ	S_ϕ	$S_{d\phi}$
dissipation rate ϵ	ϵ	$\cdot$	$\dfrac{\mu_{eff}}{\sigma_{\epsilon,eff}}$	$(C_1 G_k - C_2 \rho\epsilon) + \rho\epsilon \nabla \cdot U$	$-\dot{m}_d \epsilon$
mixture fraction	f	ρ	$\dfrac{\mu}{\sigma_f}$	0	$-\dot{m}_d (1 - f)$
fuel mass fraction	m_{fu}	ρ	$\dfrac{\mu}{\sigma_{m_{fu}}}$	$R_{chem, fu}$	$-\dot{m}_d (1 - m_{fu})$
CO mass fraction	m_{CO}	ρ	$\dfrac{\mu}{\sigma_{m_{CO}}}$	$J_{FU,CO}\, R_{chem,fu} + R_{ch,CO}$	$-\dot{m}_d\, m_{CO}$
enthalpy	$\tilde{h}$	ρ	$\dfrac{\mu}{\sigma_n}$	$\dfrac{\partial p}{\partial t} + 2a (R_x + R_y + R_z - 3E)$	$\dot{m}_d (\tilde{h}_d - \tilde{h})$
x-radiation flux	R_x	0	$\dfrac{1}{a+s}$	$-\{a (R_x - E) + \dfrac{s}{3} (2 R_x - R_y - R_z)\}$	0
y-radiation flux	R_y	0	$\dfrac{1}{a+s+\frac{1}{r}}$	$-\{a (R_y - E) + \dfrac{s}{3} (2 R_y - R_x - R_z)\}$	0
z-radiation flux	R_z	0	$\dfrac{1}{a+s}$	$-\{a (R_z - E) + \dfrac{s}{3} (2 R_z - R_x - R_y)\}$	0

In the above equation ϕ identifies the dependent variable; β is identically equal to either the mixture density ρ or zero; Γ_ϕ is the appropriate exchange coefficient for the variable ϕ; and S_ϕ is the source term which includes both the sources of ϕ (positive or negative) and any other terms which cannot find a place on the left-hand side of the equation. Table 3.8-1 summarizes the equations in the form they are solved for. Some notes about these equations now follow:

- For laminar flows, instantaneous values of flow variables and molecular values of the exchange coefficients are used.

- For turbulent flows, time-averaging values of flow variables and effective values of the exchange coefficients must be employed.

The interphase transfer source terms $S_{d\phi}$ will be discussed in chapter 4.6.

3.9 Basic Lagrangean Equations

3.9.1 Introduction

Drop life histories must be calculated in order to determine heat, mass, and momentum transfer. This is particularly important for pressure atomized injectors, where a significant proportion of the initial momentum in the flow is carried by the liquid phase and is transferred to the gas phase only by the drag force on drops. Since spray calculations are complex, the computation of droplet characteristics is represented in a relatively simple model. Droplets are assumed to be spherical and non-deformative with uniform conditions within each droplet volume. The droplets are divided into a number of drop size ranges and a system of differential equations is solved for each range.

This chapter presents basic equations of droplet motion, heat and mass transfer.

3.9.2 Droplet Distribution Model

The present model assumes that the fuel is injected into the combustion chamber as a fully atomized spray which consists of spherical droplets. The droplet-size distribution within the spray is represented by a finite number of droplet parcels of specific droplet diameter. At the atomization point droplet initial sizes, velocities and temperatures are specified; these are subsequently tracked in a Lagrangean fashion as they traverse, heat-up

and vaporize within the combustion chamber.

The number of droplets in each parcel, N_d, is calculated according to a specified distribution function, that relates the probability P_j of finding a droplet of diameter d_j to the droplet diameter:

$$N_d = \frac{\delta m_i \, P_j}{NS \sum_{j=1} P_j \, \rho_{\ell} \, \pi \, d_j^3/6} \qquad (3.9-1)$$

where NS is the number of droplet sizes and δm_i is the mass of fuel introduced at the injection location.

The most commonly used distribution function is a Rosin-Rammler function (Reference 15) (Figure 3.9-1) defined as:

$$P_R = a \, \frac{dD}{\overline{D}} \, \left(\frac{D}{\overline{D}}\right)^{a-1} \exp\left(-\left(\frac{D}{\overline{D}}\right)^a\right) \qquad (3.9-2)$$

where a is an empirical parameter (typically $1.5 < a < 3$) and $\overline{D}$ is the main droplet diameter.
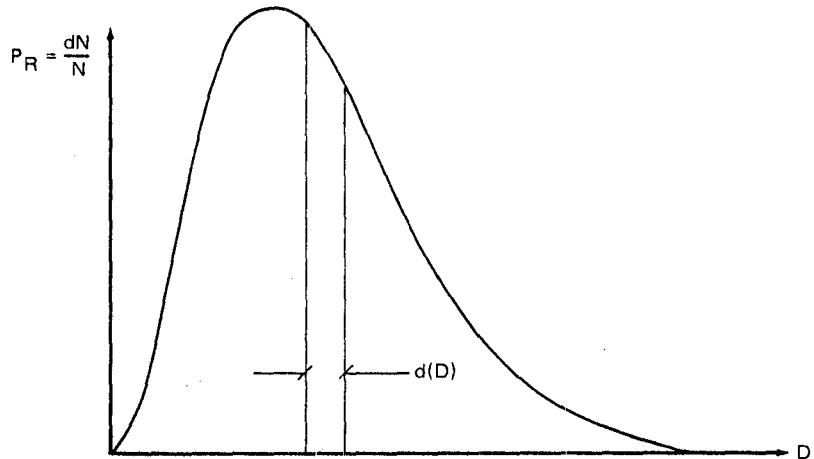

Figure 3.9-1. Droplet Size Distribution Function

The above consideration implies that the droplet trajectory, as well as heat and mass transfer within the spray, can be determined from the solution of a set of ordinary differential equations describing the behavior of each droplet parcel; these are given below.

3.9.3 Droplet Trajectory

For each droplet size the momentum balance equations are written as (References 16, 17):

$$m_d \frac{du_d}{dt} = C_D \, \rho \, \frac{A_d}{2} \, (u - u_d) \, |u - u_d|$$

$$m_d \frac{dv_d}{dt} = C_D \, \rho \, \frac{A_d}{2} \, (v - v_d) \, |v - v_d| + m_d \frac{w_d^2}{r} \qquad (3.9\text{-}3)$$

$$m_d \frac{dw_d}{dt} = C_D \, \rho \, \frac{A_d}{2} \, (w - w_d) \, |w - w_d| + m_d \frac{v_d}{r} w_d$$

Where C_D is the drag coefficient, u, v, w are gas velocity components, u_d, v_d, w_d are droplet velocity components, A_d is the droplet cross-section area, m_d is the droplet mass and r is the droplet raidal position.

The other terms contributing to aerodynamic forces on the droplet include:

- pressure gradient;
- Magnuss force;
- Saffman lift force;
- Basset force; and
- gravity forces, etc.

These are all neglected because they are of the order of gas/droplet density ratio.

The drag coefficients C_D depends primarily on the "relative" Reynolds number:

$$Re = \frac{\rho \cdot D \cdot |\bar{U} - \bar{U}_d|}{\mu} \qquad (3.9\text{-}4)$$

where D is the droplet diameter. For evaporating droplets, C_D can be calculated from the formula (References 18, 19):

$$C_D = \frac{Re}{24} (1 - 0.15 \, Re^{0.687}) \, / \, (1 + B) \qquad (3.9\text{-}5)$$

for Re up to 1000. The Spalding (transfer) number B, given by:

$$B = C_v \frac{\Delta T}{Q_L} \qquad (3.9\text{-}6)$$

3-26

can be significant for burning solid fuel particles. For evaporating droplets B is close to unity. In the above equation, C_v is the specific heat of diffusing vapor, ΔT is temperature difference, and Q_L is the latent heat of vaporization.

If droplet velocities are established, the droplet trajectory (x_d, y_d, z_d) can be obtained from simple relations:

$$\frac{dx_d}{dt} = u_d, \qquad \frac{dy_d}{dt} = v_d, \qquad \frac{dr_\theta}{dt} = w_d \qquad\qquad (3.9\text{-}7)$$

3.9.4 Droplet Heat Transfer Equation

The vaporization process for a droplet moving in a high temperature gas stream is described in terms of two regimes:

- heat-up period with raising droplet temperature, T_d; and
- equilibrium vaporization period with constant T_d.

A sketch of the droplet evaporation process is shown in Figure 3.9-2.

INJECTION INSTANCE   LATER IN LIFETIME
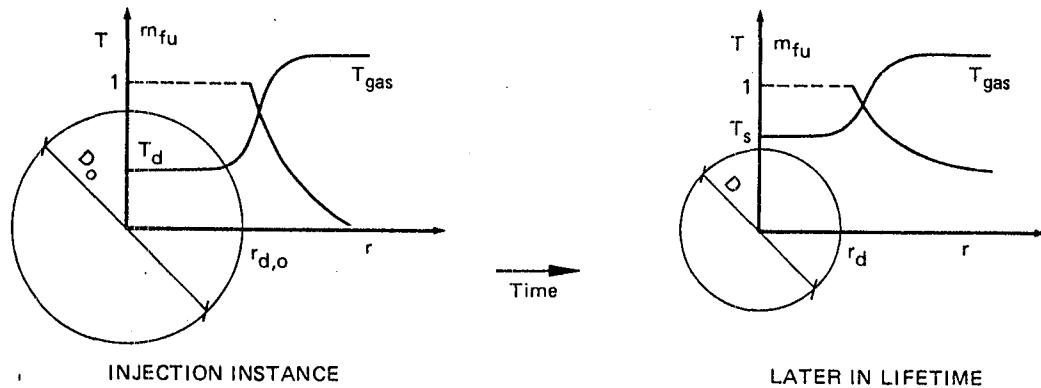
Figure 3.9-2. Sketch of the Droplet Heat and Mass Transfer During the Vaporization Process

At typical injection temperatures, the fuel concentration at the droplet surface is low and there is negligible mass transfer between the phases. As the liquid temperature rises the rate of mass transfer rises too, with the maximum liquid temperature occuring at the surface. Later in the process, due to the heat absorption for vaporization process, the droplet temperature reaches the so called "wet bulb temperature" which is almost uniform within the droplet mass.

At this stage intensive evaporation takes place with the temperature remaining constant at T_d. These two regimes are accounted for in the mathematical model of the drop heat and mass transfer processes.

Assuming quasi-steady state conditions, uniform conditions within the droplet volume and spherical shape of the droplet, the heat transfer process can be described by the following equation (References 20, 21, 22).

$$\frac{d\,T_d}{dt} = \frac{6}{D\,\rho_d\,C_d} \quad (Nu \cdot K\,(T - T_d) - \sigma a \omega\,(T_{wall}^4 - T_d^4) - Q_L) \tag{3.9-8}$$

where $Nu = 2 + .06\,Re^{0.5}\,Pr^{0.33}$ \hfill (3.9-9)

$$Q_L = L\,\frac{d\,m_d}{dt} \tag{3.9-10}$$

Here, T_d is the droplet temperature; K, C_d and L are thermal conductivity, specific heat of the liquid and latent heat of vaporization, respectively; Q_L represents the rate of the energy transfer with the evaporating mass, σ, a and ω are the Bolzman constant, droplet absorptivity and the view factor; T_{wall} is the average wall temperature. The $6/\rho_d D$ factor represents droplet area to mass ratio.

The rate of mass transfer dm_p/dt is calculated from the droplet evaporation model which is described in the next section.

3.9.5 Droplet Evaporation Model

Many single droplet and spray evaporation models exist (see for instance References 23, 24, 25). The droplet dimunition rate is conventionally expressed by:

$$\frac{d\,m_d}{dt} = \pi D \cdot K \tag{3.9-11}$$

where D is the droplet diameter and K is the evaporation constant (Reference 25).

For computational purposes, equation (3.9-11) can be rewritten in terms of

rate of decrease of droplet diameter:

$$\frac{d (D)}{dt} = \frac{2}{\rho D} K \tag{3.9-12}$$

The basic formula for the evaporation rate constant is expressed as (References 25, 26):

$$K = Sh \cdot (\rho_v K_D) (m_v - m_{v\infty}) \tag{3.9-13}$$

where Sh is the Sherwood number, K_D is the diffusion coefficient, m_v the mass fraction of vapor at the droplet surface, and $m_{v\infty}$ the mass fraction of vapor in the free stream. The Sherwood number is calculated from the Ranz and Marshal (Reference 27) formula:

$$Sh = 2 + .6 Re^{0.5} Sc^{0.33} \tag{3.9-14}$$

For the high transfer rates Sh is modified by the convection factor and is expressed as:

$$Sh = (2 + .6 Re^{0.5} Sc^{0.33}) \cdot \frac{B}{1+B} \tag{3.9-15}$$

where B is the Spalding (transfer) number, given by:

$$B = \frac{C_d (T - T_{sat})}{L} \tag{3.9-16}$$

and where C_d is the vapor specific heat and T_{sat} is the wet bulb absolute temperature.

3.9.6 Droplet-Wall Interaction

The treatment of droplets impinging on the combustion chamber walls is one of the important difficulties in modeling spray flames. If the droplet hits the solid wall, a number of possibilities exist, e.g. the droplet may shatter into small ones which become re-entrained or it may adhere in the form of the sphere or a thin film, which subsequently evaporates. In the present method it is assumed that droplets adhere at the point of impact in spherical form, and that the heat and mass transfer processes continue to obey equations (3.9-8) and (3.9-12). It is recognized however that refinement of this approach will ultimately be necessary.

4. THE NUMERICAL SOLUTION PROCEDURE

4.1 Introduction

The system of coupled nonlinear partial differential equations (PDE) and ordinary differential equations (ODE) described in the preceding chapter can only be solved by numerical methods.

This section presents numerical techniques employed for solution of both PDE (Eulerian equations) and ODE (Lagrangean equations) types.

The finite-difference technique and a modified form of SIMPLE algorithm (Reference 28, 29) are used for solution of the gas phase Eulerian equations. The resulting system of algebraic equations is then solved by efficient equation solvers.

The ODE equations describing the droplet behavior are first integrated analytically with the quasi-steady state assumption. The integration process is carried for each droplet class separately along its trajectory. During this process interphase transfer source terms for the gas-phase equations are calculated. This section describes both PDE and ODE solution practices in a detailed manner. First, however, geometry representation and space subdivision practice are presented.

4.2 Geometry and Computational Grid

4.2.1 Coordinates and Grid Lines

The REFLAN3D code can handle both cartesian and cylindrical-polar coordinates in both orthogonal and non-orthogonal form. A non-orthogonality can be simulated only in the radial direction on the x-y (x-r) plane. The code has also built-in moving grid options for simulating reciprocal processes (compressors, I.C. engines, etc.).

The coordinate systems considered are:

- x-y-z cartesian coordinates (Figure 4.1); and
- x-r-θ cylindrical polar coordinates (Figure 4.2).
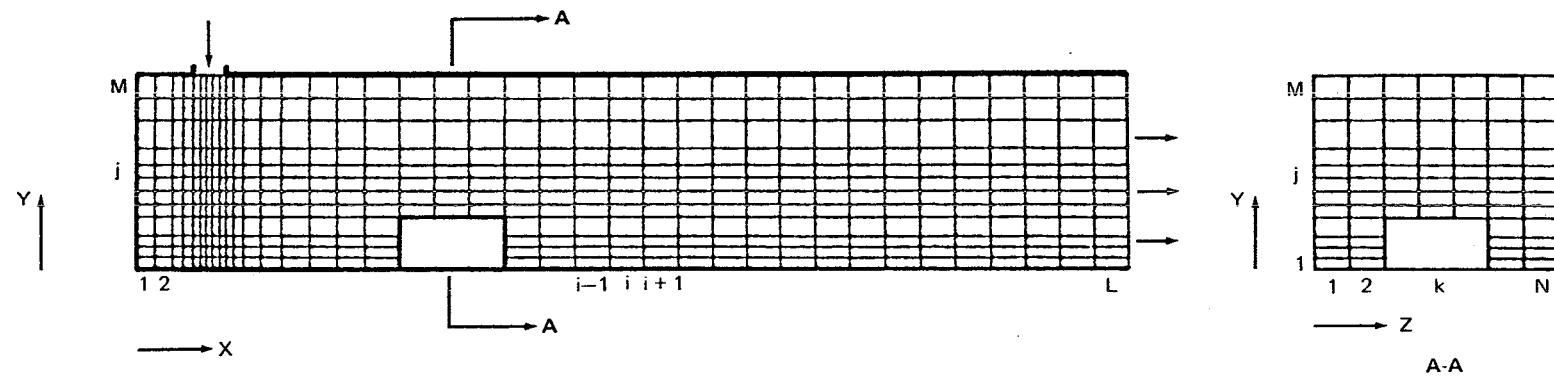
Figure 4.2   Example of the Grid Distribution in Cylindrical-Polar Coordinates
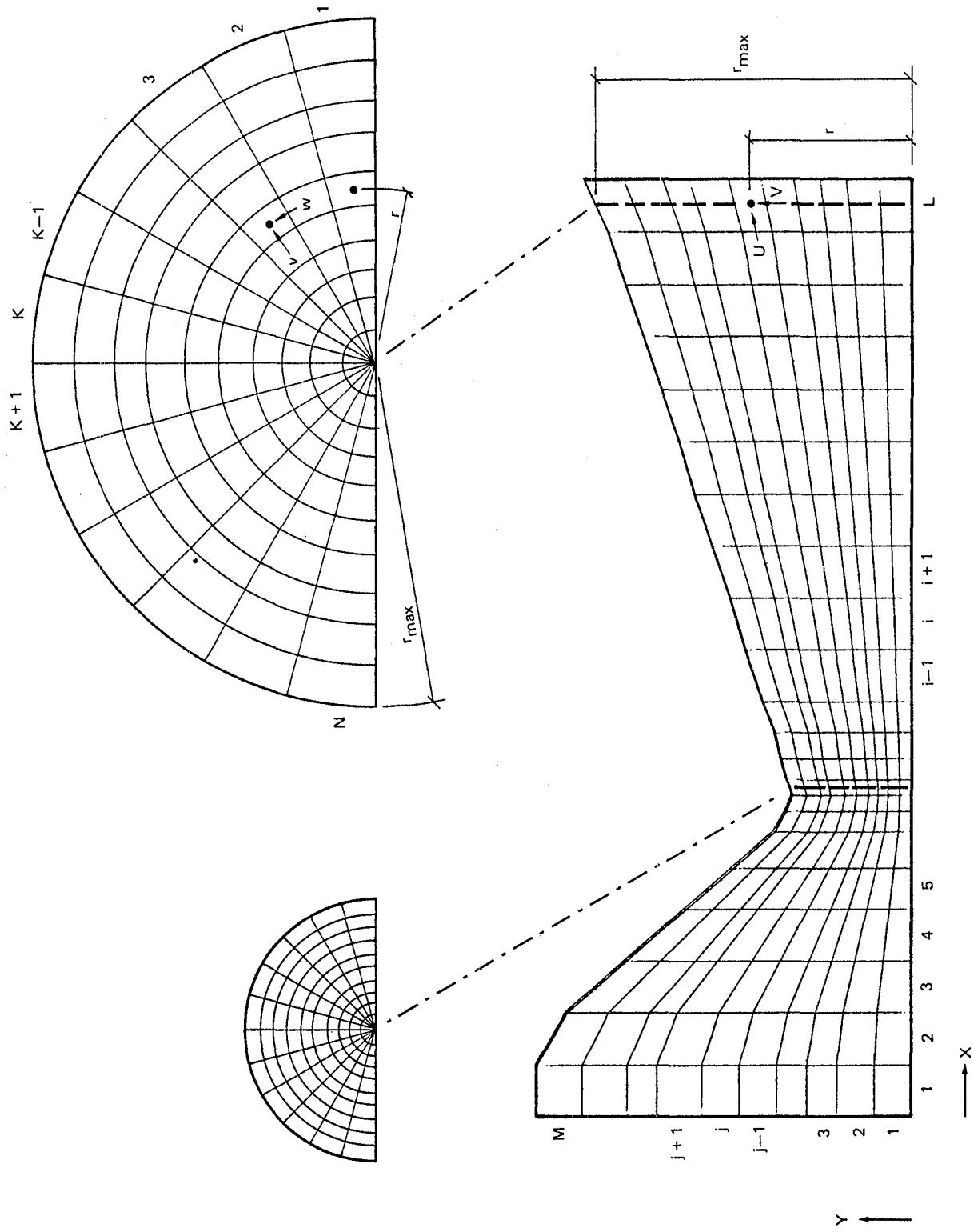
Figure 4.3. Nonorthogonal Grid Distribution for a Typical Nozzel Geometry

4-2a

For cylindrical coordinates y = 0 does not necessarily coincide with the axis of symmetry, i.e. the radius r and radial distance y at any point may differ by a constant.

The finite difference grid is formed by three sets of surfaces; perpendicular to coordinate directions. The nonorthogonal grid is formed by "piece-wise" surfaces combining r/r_{max} points in the x-y (x-r) plane (Figure 4.3). The grid distribution can be nonuniform in each coordinate direction.

4.2.2   The Staggered Grid Practice

The REFLAN3D code employs the so-called staggered grid practice (References 30, 31), in which all variables except velocities are calculated at the grid nodes (centers of the control volumes) (Figure 4.4). The velocity components are calculated at the cell faces of the control volume (designated by arrows in the diagram). A "backward boomerang" arrangement in the code implies that the velocities placed at west, south and low cell faces are assigned to each i, j, k node. The appropriate grid cell areas are also staggered in a "backward boomerang" fashion and for each node (i,j,k) calculated as A_W, A_S and A_L for x, y and z, respectively (Figure 4.4).

The derivation of the finite-difference equations will be illustrated in the first instance for a scalar variable, using the "finite volume" approach employed by Spalding (Reference 32). The porosity technique, used for representing complex geometries, allows any control volume to be fully open, partially open or fully blocked. The porosity concept is presented in the following section.

4.2.3   Porosity Concept

In many engineering problems the boundaries of the domain are irregular. Also, there can be internal flow obstacles. In most of the known approaches complex curvilinear orthogonal body-fitted coordinates are used (References 33, 34, 35) or nonorthogonal coordinates for simple geometry configurations are generated (Reference 36). The "finite domain" technique employs the so called "porosity concept" for simulating complex geometries. In this method every sub-domain is characterized by a set of volume (β_V) and cell face area (β_A)
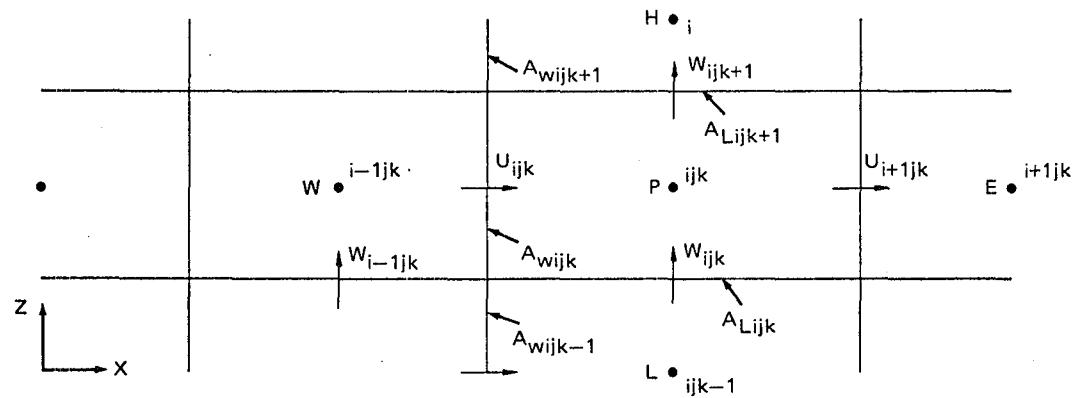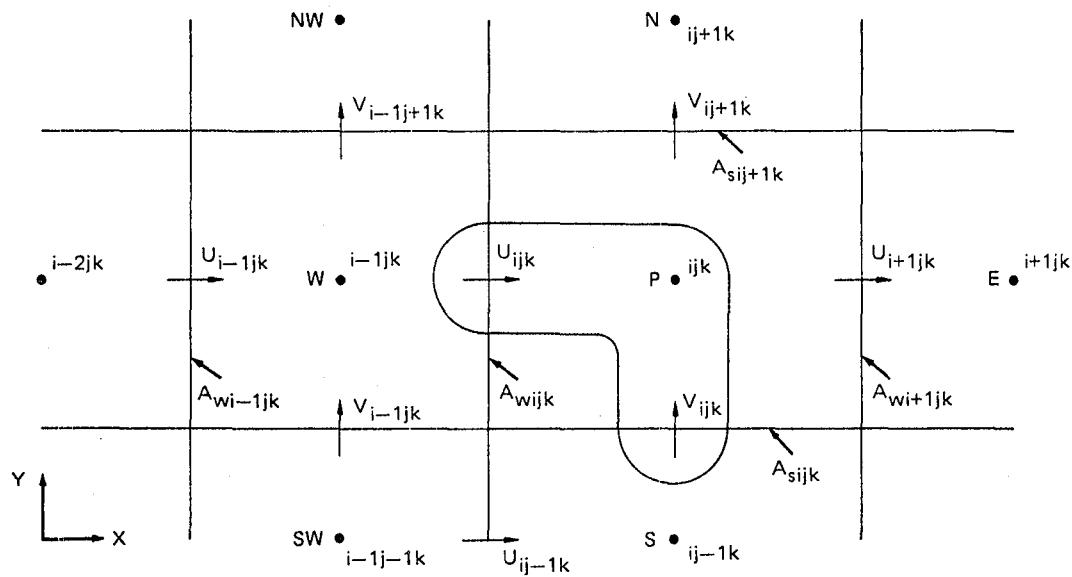
Figure 4.4   Staggered Grid Notation
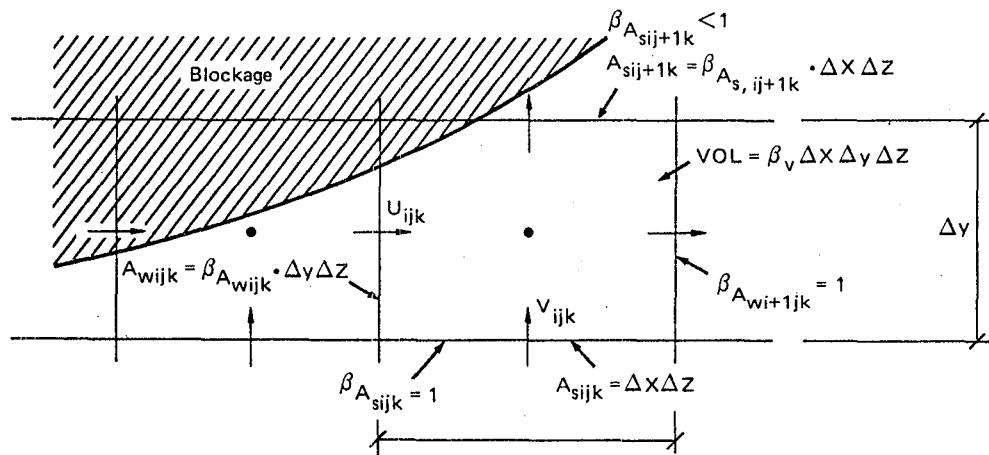
Figure 4.5   Representation of the Porosity Concept

fractions (cell porosities are usually: $0 \leq \beta \leq 1$) that are available to the fluid flow. In Figure 4.5 a typical calculation domain of the flow over an obstacle is presented. In the present case finite porosities $0 \leq \beta < 1$ are specified within and around an obstacle.

$\beta_V = 1$ for fully open volume

$0 < \beta_V < 1$ for partially blocked volume

$\beta = 0$ for fully blocked volume

A sample of a control volume within the blocked region is presented in Figure 4.5a. The volume $\beta_V V$ is used for gas flow calculations. A similar rule applies for the area porosities β_{AW}, β_{AS}, β_{AL}.

4.3   Finite Difference Equations

4.3.1   Motive of the Method

The Finite Difference Equations (FDE) are obtained by integrating the Partial Differential Equations (PDE) over the finite volume (grid cell) and, for the transient equations, over the finite time interval. The following practices have been adopted for the spatial integration of the PDE's.

- The flow variables stored at grid points are assumed to have stepwise profiles.

- The "Upwind Differencing" (UD) (References 28, 29, 37) practice is employed for integrating convective terms. This implies that the scalar flow property required at the cell face is taken equal to that at the upstream grid point.

- The cell-face velocity is considered as a cell-face average. No velocity interpolation is required for the calculation of each mass flux across the cell face.

- Fully conservative formulation is used for the integration of each quasilinear PDE. This implies that all variables within the iteration cycle are solved with the same (continuity preserving) fluxes.

For the time integration of the PDE's a fully implicit formulation is employed, i.e. the values of flow variables are taken to be those which prevail at the current time step.

A seven-node finite-difference relation will now be derived connecting the value of a dependent variable ϕ_p at the node P (Figure 4.6) with those at the E, W, N, S, H and L neighbor nodes. Integration of the PDE will result in a linear formula of the form:

$$a_p\phi_p = a_E\phi_E + a_W\phi_W + a_N\phi_N + a_S\phi_S + a_H\phi_H + a_L\phi_L + SU_\phi \qquad (4.3\text{-}1)$$

where a_E, a_W, ..., etc. are called "link coefficients", SU and SP are the linearized sources and are given by:

$$a_p = a_E + a_W + a_N + a_S + a_H + a_L - SP_\phi \qquad (4.3\text{-}2)$$

is called the main (diagonal) coefficient. All the a's, SU and SP are treated as constants.
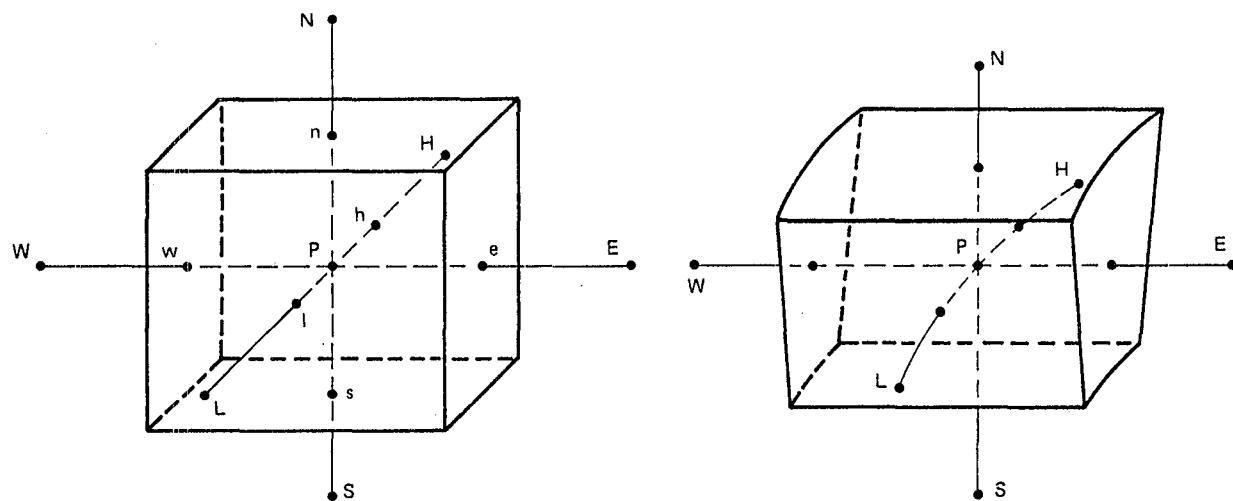

Figure 4.6. Control Volume Notation for Cartesian and Cylindrical Polar Coordinates

There will be a set of equations like (4.3-1), each with individual coefficients, for every grid point and for each of the dependent variables.

For a single variable a system of algebraic equations will be created which, in the matrix form, can be expressed as:

$$\underline{\underline{A}}\ \underline{\phi} = \underline{S} \qquad\qquad (4.3\text{-}3)$$

The system can be illustrated on an example 5:3:4 (L:M:N) grid (Figure 4.7), viz:
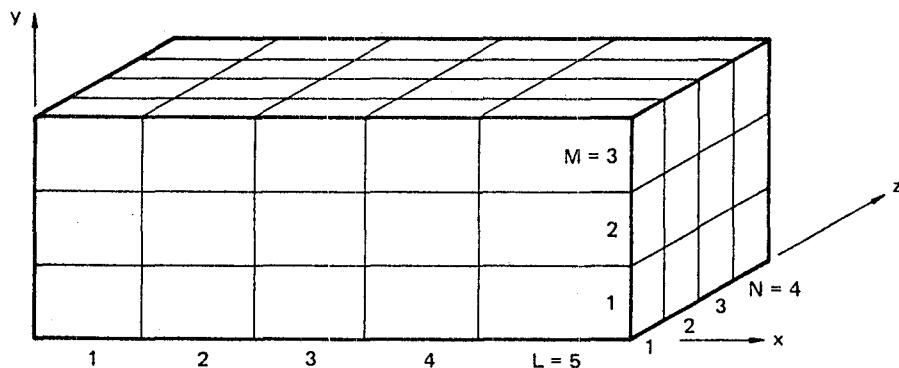
Figure 4.7. Interpretation of the Storage Allocation for Three-Dimensional Computational Domain

The corresponding matrix $\underline{\underline{A}}$ to Figure 4.7 is presented in Figure 4.8. Each dot represents non-zero link coefficients. Diagonal lines filled with squares present link coefficients for the Z-cyclic (periodic) boundary conditions.

Detailed discussion of the matrix inversion technique is discussed in Chapter 4.5. First, however, it is necessary to obtain expressions for the finite difference link coefficients (elements of matrix A in Equation 4.3-3) by integrating general transport equation in the form:

$$\underbrace{\frac{\partial \rho\phi}{\partial t} + \frac{\partial}{\partial x}\,(\rho u\phi) + \frac{1}{r}\frac{\partial}{\partial r}\,(r\rho v\phi) + \frac{1}{r}\frac{\partial}{\partial \theta}\,(\rho w\phi)}_{\text{convection terms}}$$

$$\underbrace{-\frac{\partial}{\partial x}(\Gamma_\phi\,\frac{\partial\phi}{\partial x}) - \frac{1}{r}\frac{\partial}{\partial r}\,(r\Gamma_\phi\,\frac{\partial\phi}{\partial r}) - \frac{1}{r}\frac{\partial}{\partial \theta}\,(\Gamma_\phi\,\frac{1}{r}\frac{\partial\phi}{\partial \theta})}_{\text{diffusion terms}} = \underbrace{S_\phi}_{\substack{\text{source}\\\text{term}}} \qquad (4.3\text{-}4)$$
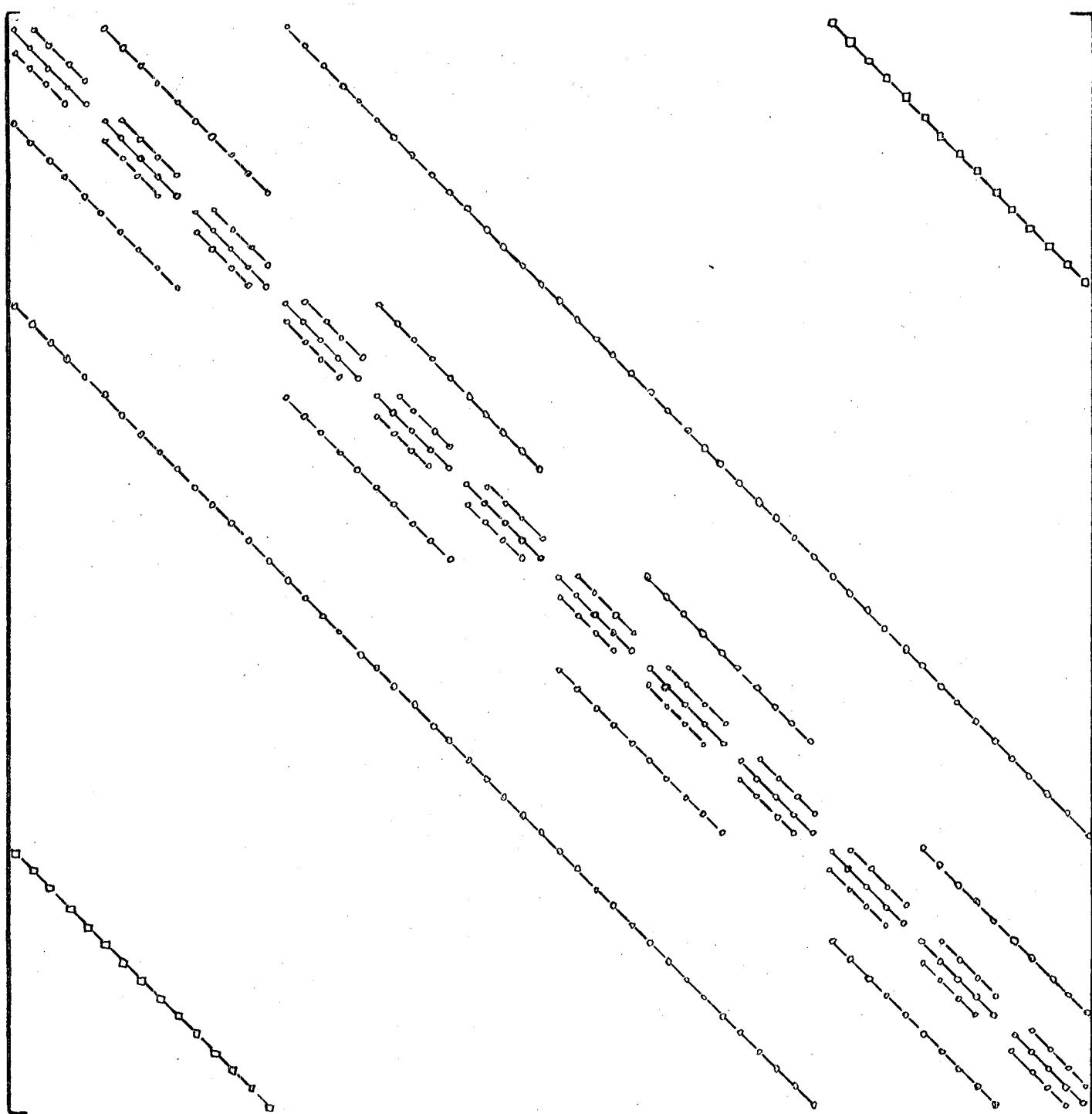
Figure 4.8   Structure of the Influence Matrix for the Three-Dimensional Calculation
Domain (see Figure 4.7)

—o—o—o—o—o— Nonzero Elements
—□—□—□—□—□— Cyclic Boundary Condition Links

The integration is discussed in the next section.

4.3.2 Integration Over a Control Volume

In order to present the derivations of the finite-difference equations, first, the x-direction related terms (equation 4.3-5) are discussed.

$$\frac{\partial \rho \phi}{\partial t} + \frac{\partial}{\partial x} (\rho u \phi) = \frac{\partial}{\partial x} (\Gamma_\phi \frac{\partial \phi}{\partial x}) + S_\phi \qquad (4.3-5)$$

Then, a generalization to three-dimensional form is provided. Figure 4.9 shows a grid node P and its x-direction neighbors W and E.
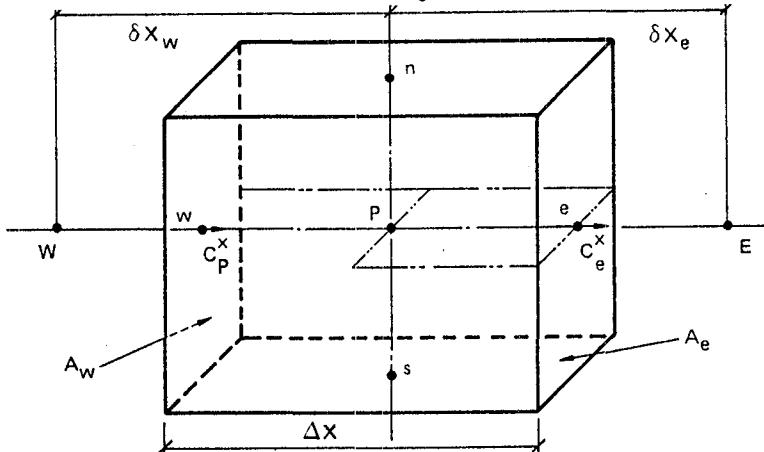
Figure 4.9. Control Volume and Notation for a One-Dimensional Transport Equation Integration

The rectangular region represents the control volume used for the integration. At the w- and e-cell faces, convective fluxes C_w^X and C_e^X are defined as:

$$C_w^X = (\rho u A)_w \text{ and } C_e^X = (\rho u A)_e \qquad (4.3-6)$$

where ρ is an "upwind" density:

$$\rho_w = \begin{cases} \rho_W: & \text{if } u_w \geq 0 \\ \\ \rho_P: & \text{if } u_w < 0 \end{cases} \qquad (4.3-7)$$

and the A's represent cell face area, i.e.

$$A_w = \begin{cases} \Delta y \Delta z & \text{for cartesian coordinates} \\ \\ r \Delta r \Delta \theta & \text{for cylindrical-polar coordinates} \end{cases} \qquad (4.3-8)$$

4-9

Integration of equation (4.3-5) in time and once in space yields:

$$\frac{(\rho\phi \text{ VOL}) - (\rho\phi \text{ VOL})^0}{\Delta t} + (\rho u\phi A)_e - (\rho u\phi A)_w +$$

$$- \left\{ (A \cdot \Gamma_\phi \frac{\partial\phi}{\partial x})_e - (A \cdot \Gamma_\phi \frac{\partial\phi}{\partial x})_w \right\} = S_\phi \cdot \text{VOL} \qquad (4.3-9)$$

Derivatives in the diffusion terms (in curly brackets) can be replaced by the appropriate finite-difference formulae:

$$(A\Gamma_\phi \frac{\partial\phi}{\partial x})_e \simeq A_e \, \Gamma_{\phi e} \frac{\phi_E - \phi_P}{\delta X_E} = D_e \, (\phi_E - \phi_P) \qquad (4.3-10)$$

and

$$(A\Gamma_\phi \frac{\partial\phi}{\partial x})_w \simeq A_w \, \Gamma_{\phi w} \frac{\phi_P - \phi_W}{\delta X_P} = D_w \, (\phi_P - \phi_W) \qquad (4.3-11)$$

where $D_e \equiv A_e \, \Gamma_{\phi e}/\delta X_E$ and $D_w \equiv A_w \, \Gamma_{\phi w}/\delta X_W$ are called "diffusion link coefficients".

The $\Gamma_{\phi e}$ and $\Gamma_{\phi w}$ are calculated from appropriate linear interpolations between the node point values. The source term S_ϕ , whenever possible, is linearized in the form:

$$S_\phi \cdot \text{VOL} = SU_\phi + SP_\phi \cdot \phi \qquad (4.3-12)$$

The upwind differencing practice is employed for approximating convective terms:

$$(\rho u\phi A)_e \simeq C_e \cdot \begin{cases} \phi_P & \text{if } C_e \geq 0 \\[2mm] \phi_E & \text{if } C_e < 0 \end{cases}$$

$$\qquad (4.3-13)$$

$$(\rho u\phi A)_w \simeq C_w \cdot \begin{cases} \phi_P & \text{if } C_w < 0 \\[2mm] \phi_W & \text{if } C_w \geq 0 \end{cases}$$

which can be rewritten using the following notation:

$$[\![a,b]\!] \equiv \max (a,b) \qquad (4.3-14)$$

$$\text{as } (\rho u\phi A)_e \simeq [\![0, C_e]\!] \, \phi_P + [\![0, -C_e]\!] \, \phi_E$$

$$\qquad (4.3-15)$$

$$\text{and } (\rho u\phi A)_w \simeq [\![0, C_w]\!] \, \phi_W + [\![0, -C_w]\!] \, \phi_W$$

Finally, equation (4.3-9) becomes:

$$\dot{M}_\phi - \overset{\circ}{M}{}^O \phi_P^O + [\![0, \; C_e]\!] \; \phi_P + [\![0, \; -C_e]\!] \; \phi_E - [\![0, \; C_w]\!] \; \phi_W - [\![0, \; -C_w]\!] \; \phi_P$$

$$(4.3\text{-}16)$$

$$- D_e \, (\phi_E - \phi_P) + D_w \, (\phi_P - \phi_W) = SU_\phi + SP_\phi \cdot \phi_P$$

where $\dot{M} = \dfrac{\rho VOL}{\Delta t}$

$$(4.3\text{-}17)$$

and $\overset{\circ}{M}{}^O = \dfrac{\rho^O VOL^O}{\Delta t}$

The integrated equation (4.3-16), analogous to equation 4.3-1, can be written as:

$$a_P \phi_P = a_E \phi_E + a_W \phi_W + SU_\phi + \overset{\circ}{M}{}^O \phi_P^O \tag{4.3-18}$$

where $\quad a_P = \dot{M} + a_E + a_W - SP_\phi \tag{4.3-19}$

and $\quad a_E = D_e + [\![0, \; -C_e]\!] \tag{4.3-20}$

$$a_W = D_w + [\![0, \; C_w]\!] \tag{4.3-21}$$

Superscript "o" indicates "old time step" value.

The above one-dimensional treatment of the differential equation (4.3-9) can now be generalized to three-dimensional flows. Consider the finite-difference equation:

$$a_P \phi_P = a_E \phi_E + a_W \phi_W + a_N \phi_N + a_S \phi_S + a_H \phi_H + a_L \phi_L + SU_\phi + \overset{\circ}{M}{}^O \phi_P^O \tag{4.3-22}$$

The various a_i coefficients are given by:

$$a_P = a_E + a_W + a_N + a_S + a_H + a_L + \dot{M} - SP_\phi \tag{4.3-23}$$

$$a_E = D_e + [\![0, \; - C_e]\!]$$

$$a_W = D_w + [\![0, \; C_w]\!]$$

$$a_N = D_n + [\![0, \; -C_n]\!]$$

$$a_S = D_s + [\![0, \; C_s]\!] \tag{4.3-24}$$

$$a_H = D_h + [\![0, \; -C_h]\!]$$

$$a_L = D_l + [\![0, \; -C_l]\!]$$

4-11

The convective C's and diffusive D's fluxes for the y and z directions are calculated from the expressions similar to that of equations (4.3-11) and (4.3-6).

4.3.3 Modifications for Non-Orthogonality of Grid

Figure 4.10a shows an example of the computational domain with nonorthogonal grid at the downstream part of the chamber. The non-orthogonality is allowed only in the axial (x-r) plane. Figure 4.10b depicts a selected control volume of the grid in the non-orthogonal region.

The inclination of the cell face from the horizontal direction is denoted by an angle α. α varies with radius such that $\alpha = 0$ at the axis of the chamber, and $\alpha = \alpha_{max}$ at the north wall of the chamber.

The net convective flux of fluid across the inclined south face of the control cell shown in Figure 4.10 is:

$$C_s = \rho_s A_s \cdot v_p - \rho_s A_{sx} \cdot u_s \qquad (4.3-25)$$

where A_s = horizontal projection of the area of the inclined north face; and

A_{sx} = vertical projection of the inclined north face area.

A_s and A_{sx} are related to each other such that:

$$A_{sx} = A_s \cdot \tan \alpha \qquad (4.3-26)$$

The axial velocity at the south cell face u_s is calculated from a linear interpolation between the u_p, u_E, u_S and u_{SE} velocities. Similar expressions can be derived for the north face. Note that in the orthogonal regions, A_{sx} is zero and therefore equation (4.3-25) reduces to the standard convective flux.

$$C_s = \rho_s A_s v_p \qquad (4.3-27)$$
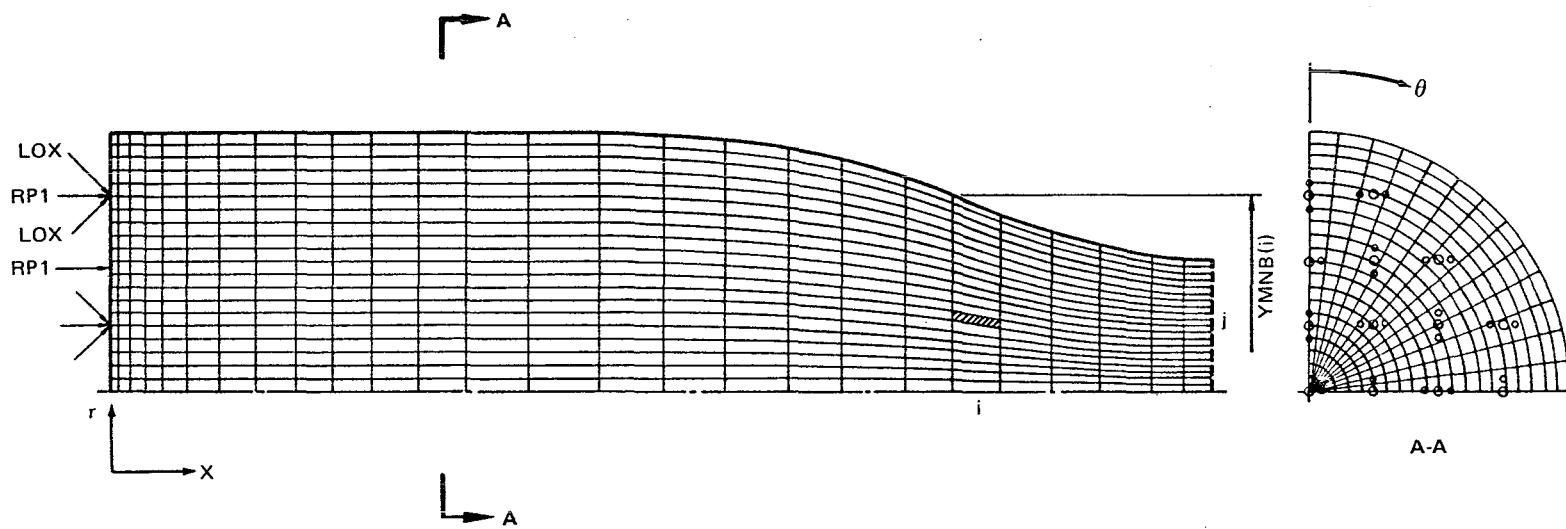
Horizontal Projection of the South Boundary Area:

$$A_s = r_{M_p} \cdot \delta\theta \cdot \delta x$$

Vertical Projection of the South Boundary Area:

$$A_{s_x} = r_{M_p} \cdot \delta\theta \cdot \delta x \cdot \tan\alpha$$
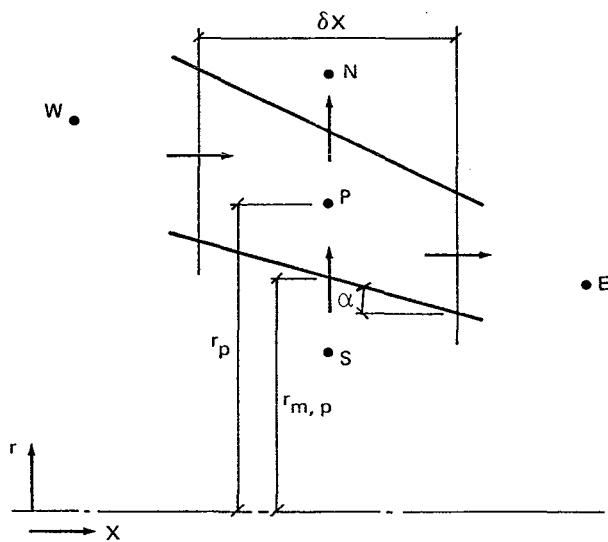
Figure 4.10. Non-Orthogonal Grid Arrangement and Nomenclature

4.3.4 The Momentum Equations

The momentum equations have a finite-difference form similar to that of the general ϕ-equation (4.3-20); but two main differences exist. First, the velocity components are at "staggered" grid locations ; therefore, the control volumes used for the velocity components are different from those for the other dependent variables. Second, the pressure-gradient term which forms a source of momentum is given a special treatment.

Figure 4.11 presents a typical control volume arrangement for the u-velocity equation integration.
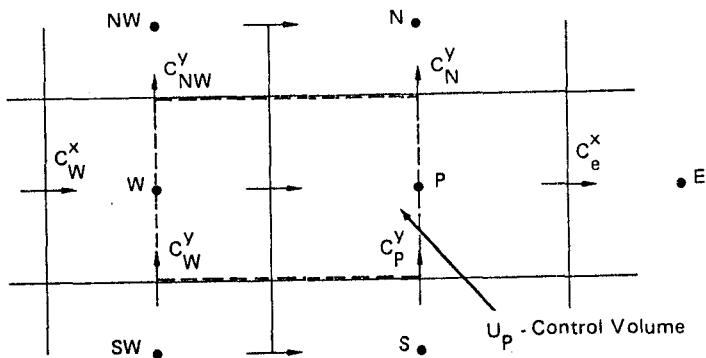
Figure 4.11. Control Volume Arrangement for Integration of u-Momentum

Note that the pressure node is always in the center of the ϕ-control volume. However, the velocity for a nonuniform grid is not necessarily placed in the middle of the u-control volume.

The finite difference equation form of the x-momentum equation is, with the pressure gradient term written out separately from other momentum sources:

$$a_p u_P = a_E u_E + a_W u_W + a_N u_N + a_S u_S + a_H u_H + a_L u_L + SU_u - A_w (p_P - p_W) + \overset{\bullet}{M}^o u_P^o$$

$$(4.3-28)$$

If velocities are solved by Jacobi iteration, it is desirable to rearrange the above equation to the following form:

$$u_P = \frac{a_E u_E + a_W u_W + a_N u_N + a_S u_S + a_H u_H + a_L u_L + SU + \overset{\bullet}{M}^o u^o}{a_p} - DU_p(P_p - P_W)$$

$$(4.3-29)$$

where:

$$DU_p \equiv \frac{A_w}{a_{p,u}}$$

$$(4.3-30)$$

The link coefficients can be written as:

$$a_P = a_E + a_W + a_N + a_S + a_H + a_L + M - SP_u$$

$$a_E = .5 \{(D_e + D_p) + [0., -c_e^x - c_p^x]\}$$

$$a_W = .5 \{(D_p + D_w) + [0, c_p^x + c_w^x]\}$$

$$a_N = .5 \{(D_n + D_{nw}) + [0., -c_n^y] + [0., -c_{nw}^y]\} \qquad (4.3\text{-}31)$$

$$a_S = .5 \{(D_S + D_{SW}) + [0., c_p^y] + [0., c_w^y]\}$$

$$a_H = .5 \{(D_h + D_p) + [0., -c_h^z] + [0., -c_{hw}^z]\}$$

$$a_L = .5 \{(D_l + D_p) + [0., c_p^z] + [0., -c_{lw}^z]\}$$

The r and θ momentum equations have similar finite difference form.

Note that the convective parts of a_N, a_S, a_H and a_L link coefficients are calculated for both convective subfluxes separately (see Figure 4.11). In the alternative approach, first a net convective flux is calculated as a sum of two subfluxes and then upwind principle is employed, e.g.:

$$a_N = .5 \{(D_n + D_{nw}) + [0., -c_n^y - c_{nw}^y]\} \qquad (4.3\text{-}32)$$

This practice is used in several existing and widely used codes, e.g. CORA3, TEACH, COM3D and STARPIC.

Figure 4.12 presents comparison between the practices for a selected flow configuration ($c_w^y + c_p^y < 0$ and $c_{NW}^y + c_N^y > 0$).

(a) REFLAN (LINKS WITH U_N, U_S and U_W)   (b) OTHER (LINKS WITH U_N and U_W ONLY)
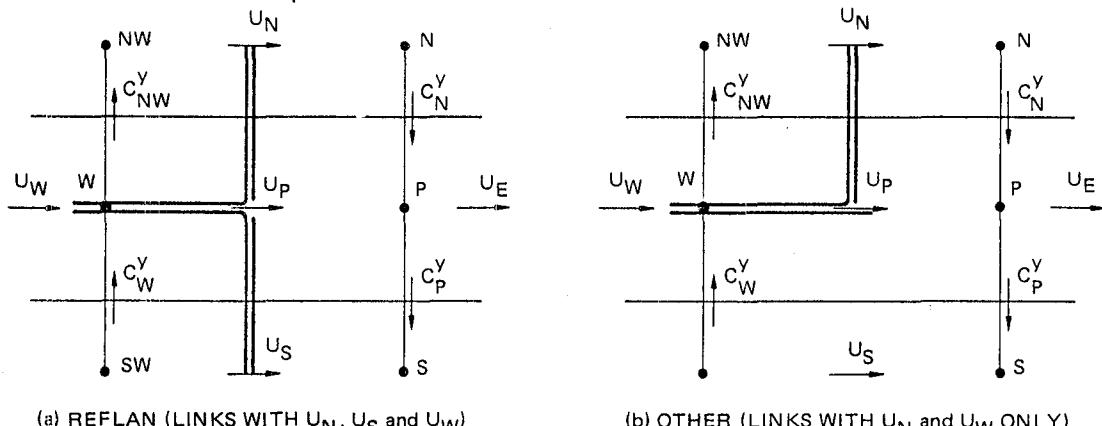
Figure 4.12. Convective Link Coefficients for U_p - Momentum Equations

In recirculation regions, the practice employed in REFLAN3D retains convective links with both North and South neighbor velocities u_N, u_S. Other practices maintain the link only with u_N.

The practice used in REFLAN3D code is based on a full conservation principle, and, by employing more links, it is also more accurate than the other practices mentioned earlier. A similar treatment yields the link coefficients for radial v and circumferential w velocity components.

The momentum equations are solved by using a modified version of the SIMPLE algorithm (Reference 28). In SIMPLE, the momentum equations are first solved with a guessed pressure distribution, denoted by p*, to give a first approximation to the velocity fields, u*, v* and w* (the starred-velocity fields). These velocities are approximate because they do not in general satisfy the continuity equation. Corrections to the pressure and velocity fields are then obtained from the solution of pressure-correction equations which are derived from the continuity equations (see Section 4.3.5 below). These corrections are such that the resulting velocities reduce continuity errors. The iterative is continued until convergence.

4.3.5   The Continuity Equation: Pressure-Correction Equation

It has been mentioned above that the velocities obtained from the momentum equations do not satisfy the continuity equation, and therefore require correction. The correction of velocities and pressure is discussed in this section.

The continuity equation is:

$$\frac{\partial}{\partial x} (\rho u) + \frac{1}{r} \frac{\partial}{\partial r} (\rho v r) + \frac{1}{r} \frac{\partial}{\partial \theta} (\rho w) = 0 \qquad (4.3\text{-}33)$$

It can be written in the finite difference form as:

$$\frac{\rho_p VOL}{\Delta t} - \frac{\rho_p^0 VOL^0}{\Delta t} + C_e^x - C_w^x + C_n^y - C_s^y + C_h^z - C_l^z = 0. \qquad (4.3-34)$$

where (to remind) $C_e^x = (\rho u A)_e, \ldots$ \qquad\qquad (4.3-35)

Again, to start with, a one-dimensional problem is considered. From the momentum equations, the following relationships are obtained:

$$u_e = u_e{}^* + DU_e \; (p_E' - p_P') \qquad\qquad (4.3-36)*$$

and

$$u_w = u_w^* + DU_w \; (p_P' - p_W') \qquad\qquad (4.3-37)*$$

Here p' is the pressure-correction, and DU's are the pressure-difference coefficients which were calculated from equation (4.3-30) during the solution of the momentum equations.

For compressible flows additional density correction is performed. The correction practice employed is based on the pressure density relation:

$$\rho = \rho^* + (\frac{\partial \rho}{\partial p}) \cdot p' \qquad\qquad (4.3-38)$$

where $(\frac{\partial \rho}{\partial p})$ is calculated from equation of state.

Substitution of ρ (4.3-38) and u (4.3-36 and 37) into the mass conservation equation (4.3-34) results in:

$$\frac{VOL}{\Delta t} (\rho^* + \frac{\partial \rho}{\partial p} P_p') - \frac{\rho_p^0 \; VOL^0}{\Delta t} + (u_e^* + DU_e \; (p_E' - p_P'))(\rho_e + \frac{\partial \rho}{\partial p} p_e') A_e +$$

$$- (u_w^* + DU_w \; (p_P' - p_W')) \; (\rho_w + \frac{\partial \rho}{\partial p} p_W') A_w + \ldots \qquad (4.3-39)$$

** Equations (4.3-36) and (4.3-37) are approximate forms of the momentum equations. The exact form would be:

$$u_e = u_e^* + DU_e \; (p_P' - p_E') + \sum_i a_i \; (u_i - u_i^*)$$

where i indicates summation over the neighboring nodes; and a_i are the finite-difference link coefficients from equation (4.3-29).

If an upwind differencing practice is used for cell-face density calculations and ignoring terms of order p'^2, the pressure correction equation can be written as follows:

$$a_p p_P' = a_E u_E + a_W u_W + a_N u_N + a_S u_S + a_H u_H + a_L u_L + SU + \dot{M}^* - \dot{M}^O \qquad (4.3\text{-}40)$$

where $a_p = \dfrac{VOL}{\Delta t} \cdot \dfrac{\partial \rho}{\partial p} + a_W + a_E + a_N + a_S + a_H + a_L$

$$a_W = \rho_w A_w DU_w + [0., U_w] A_w \cdot (\partial \rho/\partial p)_w$$

$$a_E = \rho_e A_e DU_e + [0., U_e] A_e \cdot (\partial \rho/\partial p)_e$$

$$a_N = \rho_n A_n DV_n + [0., V_n] A_n \cdot (\partial \rho/\partial p)_n \qquad (4.3\text{-}41)$$

$$a_S = \rho_s A_s DV_s + [0., V_s] A_s \cdot (\partial \rho/\partial p)_s$$

$$a_H = \rho_h A_h DW_h + [0., W_h] A_h \cdot (\partial \rho/\partial p)_h$$

$$a_L = \rho_l A_l DW_l + [0., W_l] A_l \cdot (\partial \rho/\partial p)_l$$

The source term SU represents net mass flux imbalance of the u^*, v^*, w^*-velocity field. Thus:

$$SU = C_e^{x*} - C_w^{x*} + C_n^{y*} - C_s^{y*} + C_h^{z*} - C_l^{z*} \qquad (4.3\text{-}42)$$

The purpose of the pressure-correction equation is to reduce this mass source to zero. When these sources are everywhere zero, the solution is just $p' = 0$.

After solving equation (4.3-40) the corrected velocities are obtained from equations (4.3-36) and (4.3-37). (Similar equations hold for the v- and w-velocities.) Density is corrected via equation (4.3-30), and pressure, from:

$$p = p^* + p' \qquad (4.3\text{-}43)$$

In the derivation of equation (4.3-40), the approximate form of the momentum equation has been used. However, no error is thereby introduced. In a converged solution for a steady-state problem, the mass-sources and the pressure corrections will have become zero (in reality, a relatively small number) in the final iteration so that the solution is independent of what actually went into the derivation of the pressure-correction equation.

Note that after solving p', correcting velocities and calculating new, continuity obeying, convective fluxes the remaining equations k, ε, $\tilde{h}$ ... , etc. can be solved in a fully conservative formulation.

4.4   The Radiation-Flux Equations

The differential equations for the three composite radiation fluxes R_x, R_y and R_z, equation (3.6-4) is much simpler than the general equation (3.8-1). The equation for the x-direction flux R_x can be written as:

$$\frac{d}{dx}\left(\Gamma \frac{dR_x}{dx}\right) + S = 0 \tag{4.4-1}$$

where $\Gamma = 1/(a+s)$ (4.4-2)

and $S = a(R_x - E) + s(R_x - R_y)/2$ (4.4-3)

The finite difference form of this equation is obtained by integration over the x-direction length of the control volume. The integral of the source term S is expressed as $(SU + SP . R_{xp})$ as before, and the complete finite-difference equation can be written as:

$$a_P\, R_{xp} = a_W\, R_{x_e} + a_W\, R_{x_w} + SU \tag{4.4-4}$$

where $a_P \equiv a_W + a_E - SP$

   $a_W \equiv \Gamma_e/\sigma x_e$ (4.4-5)

   $a_W \equiv \Gamma_w/\sigma x_w$

The distances δx_e and δx_e are defined in Figure 4.9.

Similar equations can be obtained for the y-direction and z-direction fluxes R_y and R_z, respectively.

4-19

4.5   Solution Method of the Complete Equation Set

For the NX, NY, NZ grid and NVAR dependent variables (u, v, w, p, k, ε, $\tilde{h}$ ...) to be solved for, the finite difference equation set can be written in the matrix form as:

$$As = B \tag{4.5-1}$$

where s is the solution vector containing all the unknown velocities, pressures, enthalpies, concentrations, etc., B is the "source" vector and A is the coefficient matrix of the form:
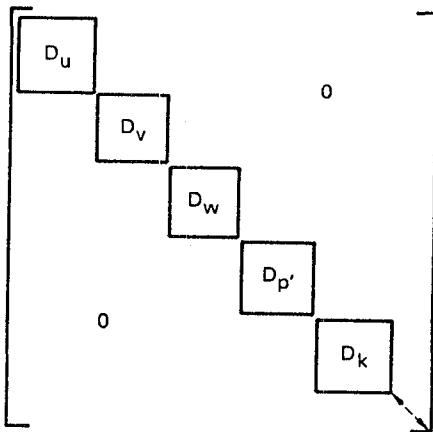
Figure 4.8. Matrix Arrangement for the Complete Equation Set

where the form of D_u, D_v, ... submatrices is as that on Figure 4.8.

It is seen that the matrix A has a large and extremely sparse structure. For a typical 3-dimensional problem with 20 x 20 x 20 grid and 10 dependent variables (80 000 algebraic equations) matrix A has 64 million elements. Of these, less than 48,000 are non-zero.

Utilization of any direct solvers, such as Gaussian elimination (Reference 40) or band solvers (Reference 41), even for much smaller systems is inpractical for the following reasons:

   a) prohibitive storage;

   b) such a solver would have to employ partial pivoting because of zeros along the diagonal;

   c) solution time of direct solvers is proportional to the number of unknowns to the power 2 to 3; and

   d) the equation system is nonlinear so that several matrix inversions would be required.

The only alternative solution algorithm is to solve the (4.3-3) equations separately for each dependent variable. Even in this case, solution of equation (4.3-3) for three-dimensional flows is a formidable task.

It has been mentioned before that the momentum equations are solved by the Jacobi, point-by-point algorithm (References 40, 42). The remaining equations including p'-equation, are solved simultaneously by the so-called "Whole Field" solution process at all control cells within the calculation domain.

The simultaneous solution practice employed in the REFLAN3D code is described in the following section.

4.5.1   The Whole Field Solution Practice

In last five years, the commonly used "Alternating Direction Implicit", ADI, method (References 38, 24) for the solution of a system of algebraic equations has been replaced by Whole Field Solvers (WFS).

Spalding and his coworkers (Reference 60, 61) have devised and used a WFS which is similar to Stone's Strongly Implicit Procedure, SIP, (Reference 44) but completely free from any adjustable (convergence-promotor) parameter called α-parameter. Subsequently Gosman and others (Reference 45 to 48) have investigated effectiveness of the WFS. All of these solvers are itenative field traverse methods involving a forward march for assembling the solver coefficients and backward march for back substitution. However due to the inconvenience of indexing practices, the marching directions are not reversed or alternated, as a result these solvers are not symmetric.

A new fully symmetric solver which is totally independent of the α-parameter has been recently developed at CHAM by Przekwas (Reference 49) and employed in the REFLAN3D code.

Figure 4.13 illustrates the grid node arrangement and the nomenclature for the WFS discussion.
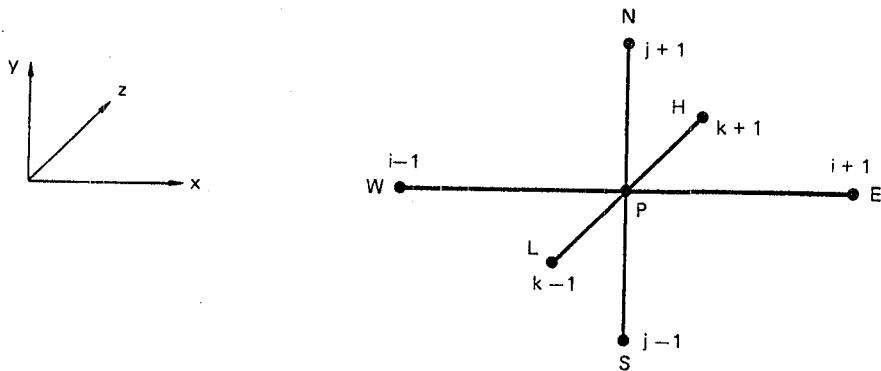
Figure 4.13. Grid Node Nomenclature for the WFS Discussion

With the i, j, k indices omitted the FD equation can be expressed as:

$$a_P \phi = a_E \phi_{i+1} + a_W \phi_{i-1} + a_N \phi_{j+1} + a_S \phi_{j-1} + a_H \phi_{k+1} + a_L \phi_{k-1} + SU \qquad (4.5-2)$$

The solution algorithm of the z-symmetric 3-D WF solver for the system of the FD equations (4.5-2) can be summarized as follows.

Forward March: i) calculate ϕ independent modified coefficients (in increasing i, j, k order)

$$E \equiv a_E/D$$

$$N \equiv a_N/D$$

$$H \equiv a_H/D$$

$$L \equiv a_L/D$$

$$D \equiv a_P - a_W E_{i-1} - a_S N_{j-1}$$

ii) calculate the modified right-hand-side (in the order as above).

$$BB = (SU + a_W (N_{i-1}\phi_{i-1,j+1} + H_{i-1}\phi_{i-1,k+1} + L_{i-1}\phi_{i-1,k-1} + BB_{i-1}) +$$

$$+ a_S (E_{j-1}\phi_{i+1,j-1} + H_{j-1}\phi_{j-1,k+1} + L_{j-1}\phi_{j-1,k-1} + BB_{j-1}))/D \qquad (4.5-4)$$

<u>Backsubstitution</u>: iii) solve tridiagonal equations (in decreasing i j order).

$$-L\phi_{k-1} + \phi - H\phi_{k+1} = BB + E\phi_{i+1} + N\phi_{j+1}$$

using TDMA or CTDMA (see next section) along each k-line.

iv) return to ii until number of sweeps or convergence criteria has been reached.

This method has an additional advantage of implicit treatment of the periodic boundary conditions in the z-direction. It is also generally faster than any of the earlier mentioned practices.

In the following section a TDMA (Tri-Diagonal Matrix Algorithm) and CTDMA (Cyclic-TDMA) are discussed. The algebraic equation (4.5-5) along any z-line (k=1 ... NZ) can be expressed in general form as:

$$A_k\phi_{k-1} + B_k\phi_k + C_k\phi_{k+1} = D_k \tag{4.5-6}$$

where $A_k = L_k$

$\qquad B_k = 1$

$\qquad C_k = H_k$ $\tag{4.5-7}$

$\qquad D_k = BB_k + E_k\phi_{i+1} + N_k\phi_{j+1}$

and can be used as a basis for the following discussion.

4.5.2 <u>The TDMA Algorithm</u>

The solution algorithm consists of two steps:

a) forward march: where the TDMA coefficients are calculated as follows:

$$\alpha_k = \frac{-C_k}{B_k + A_k\alpha_{k-1}}$$

$$\beta_k = \frac{D_k - A_k\beta_{k-1}}{B_k + A_k\alpha_{k-1}}$$

$$k = 1, 2, \ldots NZ \tag{4.5-8}$$

b) back-substitution: where ϕ values are calculated as follows:

$$\phi_{NZ} = \beta_{NZ}$$

$$\phi_k = \alpha_k \, \phi_{k+1} + \beta_k$$

$$k = NZ-1, NZ-2, \ldots, 2, 1 \qquad (4.5-9)$$

4.5.3 The CTDMA Algorithm

The Cyclic-TDMA algorithm is used to solve the system of equations with periodic (cyclic) boundary conditions. Figure 4.14 presents a grid arrangement with cyclic boundary conditions.
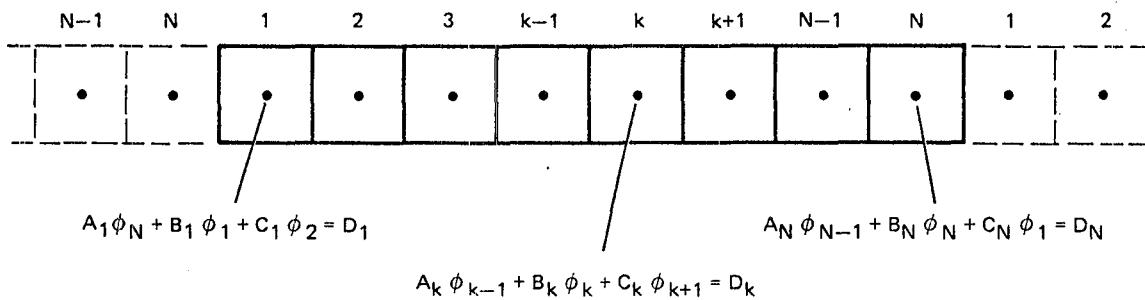
Figure 4.14. Grid Arrangement and Equation Forms for Cyclic Boundary Conditions

Note that the (k-1) neighbor of ϕ_1 is ϕ_{NZ}. Detailed description of cyclic boundary conditions is discussed in chapter 5. Here only the solution algorithm is outlined. Similarly as for TDMA the solution algorithm consists of two steps:

a) forward march - where the CTDMA coefficients are calculated as follows:

4-24

for $k = 1$

$$\alpha_1 = D_1/B_1 \qquad\qquad F = D_{NZ}$$

$$\beta_1 = C_1/B_1 \qquad \text{and} \qquad G = C_{NZ} \qquad\qquad (4.5\text{-}10)$$

$$\sigma_1 = A_1/B_1 \qquad\qquad H = B_{NZ}$$

for $k = 2, \ldots, NZ-1$

$$\alpha_k = (D_k - A_k \; \alpha_{k-1})/W_x \qquad\qquad F_k = F_{k-1} - G_{k-1}\alpha_{k-1}$$

$$\beta_k = C_k/W_w \qquad \text{and} \qquad G_k = -\beta_{k-1} \; G_{k-1} \qquad (4.5\text{-}11)$$

$$\sigma_k = A_k \circ \sigma_{k-1}/W_k \qquad\qquad H_k = H_{k-1} - G_{k-1} \; \sigma_{k-1}$$

where $\qquad a = B_k - A_k\beta_{k-1} \qquad\qquad\qquad\qquad\qquad (4.5\text{-}12)$

b) back-substitution - where ϕ values are calculated:

$$\phi_{NZ} = \frac{F_{NZ-1} - (G_{NZ-1} - A_{NZ}) \cdot \sigma_{NZ-1}}{H_{NZ-1} - (G_{NZ-1} + A_{NZ})(\beta_{NZ-1} + \sigma_{NZ-1})} \qquad (4.5\text{-}13)$$

and

$$\phi_k = \sigma_k - \beta_k \; \phi_{k+1} = \sigma_k \; \phi_{NZ} \qquad k = NZ-1, NZ-2, \ldots, 2,1 \qquad (4.5\text{-}14)$$

4.5.4 Under-Relaxation

The calculation procedure described above involves the solution of nonlinear differential equations expressed in the form of the linearized finite-difference equations. Therefore, an iterative procedure has to be applied to continuously update the coefficients until a converged solution is obtained. If the changes in the values of the variables from one iteration to the next are large, there is a possibility that convergence may not be achieved at all. To keep these changes sufficiently small, the dependent variables are suitably under-relaxed.

There are two under-relaxation practices employed:

1. inertial under-relaxation of dependent variables (u, v, k, ε ...); and

2. direct under-relaxation for secondary variables (μ, P).

Inertial under-relaxation of the dependent variables is achieved by adding an inertial term viz: $I_\phi(\phi - \phi^*)$ to the finite equation in the following manner:

$$\phi = \frac{\Sigma a_n \phi_n + SU + I_\phi \phi^*}{\Sigma a_n - SP + I_\phi} \qquad (4.5-15)$$

where suffix n denotes all cell neighbors, and supscript * denotes previous iteration value of ϕ. The "inertia term" I is calculated as:

$$I = \frac{\rho \, VOL}{\Delta t_{F\phi}} \qquad (4.5-16)$$

where ρ is the fluid density, VOL is the grid cell volume and $\Delta t_{F\phi}$ is the "false" time step specified for each dependent variable ϕ. The main features of equation (4.5-15) can be summarized as:

1. In a converged solution $\phi = \phi^*$, and therefore the final solution of the finite difference equation is not affected by the magnitude of I.

2. $\frac{\rho \, VOL}{\Delta t_{F\phi}}$ has the dimension of flow rate.

3. The smaller the value of $\Delta t_{F\phi}$, the heavier is the under-relaxation.

4. $I\phi^*$ and I are included in SU and SP components of the source term so that the general form of the equation remains as Equation 4.5-2.

The direct under-relaxation practice is implemented by calculating the under-relaxed ϕ^u-value as a weighted average of just-calculated ϕ-value and previous iteration ϕ^*-value in the form:

$$\phi^u = \alpha_\phi \phi + (1 - \alpha_\phi) \phi^* \qquad (4.5-17)$$

where α_ϕ is the under-relaxation factor for ϕ variable and has the value between zero and one ($\alpha = 1$ implies no under-relaxation).

4.5.5 Calculation of Residual Errors and Convergence Criteria

The residual errors are calculated for the equations of all dependent variables at each control cell, in the following manner:

$$\epsilon_{\phi P} = \Sigma a_n \phi_n + SU - SP \phi_P^* - (\Sigma a_n) \phi_P^* \qquad (4.5\text{-}18)$$

where $\epsilon_{\phi P}$ stands for the residual error in the equation of variable ϕ at point P, and summation is taken over all link coefficients: N, E, W, S, H, ... The above equation is obtained from equation 4.5-16 by transferring all terms to the right-hand-side and equating them to the residual error. Three major quantities can provide the information on the convergence of the solution obtained and can be printed by the REFLAN3D code at any iteration. These are:

1. Maximum residual error

$$RESMAX = \max_{ijk} (\epsilon_{\phi_{ijk}}) \qquad (4.5\text{-}19)$$

2. Global residual error

$$RESSUM = \sum_{ijk} \epsilon_{\phi_{ijk}} \qquad (4.5\text{-}20)$$

3. Global absolute residual error

$$RESSUMABS = \sum_{ijk} |\epsilon_{\phi_{ijk}}| \qquad (4.5\text{-}21)$$

Additionally an absolute difference between two consecutive iteration ϕ-values is calculated as:

$$DIFMAX = \max_{ijk} (\phi_{ijk} - \phi_{ijk}^*) \qquad (4.5\text{-}22)$$

which is searched for over the entire calculation domain.

The solution is regarded as converged when all above quantities take values below their prescribed limits. Usually it requires reduction of two, three and sometimes four orders of magnitude of the residual before this occurs.

4.6 Integration of the Lagrangean Equations

4.6.1 Integration Practice

The Lagrangean equations for the droplet motion, heat and mass transfer (see Chapter 3.9) can be expressed in a general form of ordinary differential equation (ODE) as:

$$\frac{d\,\phi_d}{dt} = \frac{1}{E}\,(\phi_g - \phi_d) + F \qquad\qquad (4.6\text{-}1)$$

where ϕ_g and ϕ_d represent gas-phase and droplet property, respectively. The E and F coefficients in general Lagrangean equation (4.6-1) can be obtained from equations governing droplet momentum (3.9-3), energy (3.9-8) and mass (3.9-11) conservation. The solution practice for the Lagrangean and Eulerian ones is totally different. The PDE's of the Eulerian part are solved as a boundary value problem while the ODE's of the Lagrangean part represent an initial value problem.

Several techniques for solving a system of coupled ODE's of the droplet behavior have been used, including integration formulae (Reference 50), second order predictor-corrector schemes (References 51, 52), and fourth order Runge-Kutta (R-K) scheme (Reference 53, 54) and analitical integration techniques (Reference 20, 21, 22).

In this study equations (4.5-1) are solved analytically. This technique offers considerable economy in computing time in comparison with the iterative fourth order R-K scheme (Reference 53).

Integration of equation (4.6-1), assuming the gas property ϕ_g is constant over the time of integration, yields:

$$\phi = \phi_g - (\phi_g - \phi_d)\,\exp\left(-\frac{\Delta t}{E}\right) + E\,F\,\left(1 - \exp\left(-\frac{\Delta t}{E}\right)\right) \qquad (4.6\text{-}2)$$

where Δt is the time interval. It is worthy to note that the E factor represents a characteristic time scale (or relaxation time) for the process. If, during the integration process, the time scale ratio $\Delta t/E$ is larger than say 20, the $\exp(-\Delta t/E)$ is smaller than 2.10^{-9} and the integration effort of equation (4.6-2) is greatly simplified.

4.6.2 Droplet Trajectory

After determining droplet velocity at time $t + \Delta t$, the droplet position at time $t + \Delta t$ is determined from:

$$\bar{x}_d = \bar{x}_d^{\ 0} + (\bar{U}_d - \bar{U}_d^{\ 0}) \frac{\Delta t}{2} \qquad (4.6\text{-}3)$$

where $\bar{x}_d^{\ 0}$ is the droplet position at the beginning of the time increment and $\bar{U}_d^{\ 0}$ is its initial velocity (at $\bar{x}_d^{\ 0}$).

Figure 4.6-1 depicts consecutive droplet positions along its trajectory crossing the orthogonal Eulerian grid cells. The integration process starts at the cell surface (position $\bar{x}_1$ in Figure 4.6-1) where cell droplet inlet properties $U_{d_{IN}}$, $V_{d_{IN}}$, $W_{d_{IN}}$, $T_{d_{IN}}$, $D_{d_{IN}}$, are solved.
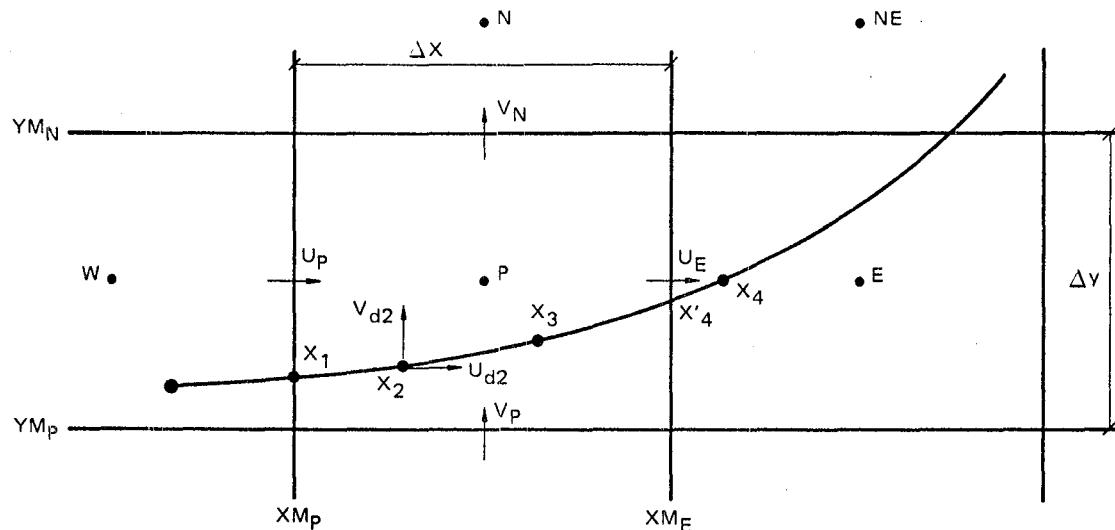
Figure 4.6-1. Droplet Trajectory Passing the Computational Cell

Next the estimate for the time interval for the integration process is calculated as:

$$\Delta t = \alpha_{INT} \cdot \min \left(\frac{(U_P + U_E)/2}{\Delta x}, \frac{(V_P + V_N)/2}{\Delta y}, \frac{U_d}{\Delta x}, \frac{V_d}{\Delta y} \right) \qquad (4.6\text{-}4)$$

where $\alpha_{INT} < 1$ is the parameter approximately specifying the number of integration interval before the droplet reaches the exit position at the grid

cell face. As an example, in uniform gas and droplet velocity field, $\alpha_{INT} = 1/5$ would imply five time steps within the grid cell.

Then the new droplet velocities, temperature and diameter are calculated from equation 4.6-1 and new droplet position is established from equation 4.6-3, (point 2 in Figure 4.6-11). Next, integration time interval Δt is calculated again and the integration process is repeated until droplet crosses the cell face (point 4 in Figure 4.6-1).

At this stage linear interpolation is employed between points 3 and 4 to find droplet properties (u_d, v_d, w_d, T_d, D_d) at the cell face (point 4 in Figure 4.6-1). A droplet exit point "Ex" has been found and the integration procedure is completed by calculating interphase sources between the liquid and gas phase. The mass transfer, for example, is calculated as:

$$\dot{m}_{INT} = \frac{\pi}{6} \rho_d \left(D^3_{dIN} - D^3_{dEX} \right) \dot{n}_d \tag{4.6-5}$$

where $\dot{n}_d$ is the number of droplets traversing the grid cell in unit time.

Detailed discussion of the interphase source calculation is discussed in the following section.

The exit droplet position in the P grid cell (point 4 in Figure 4.6-1) is considered as an entry point for E-grid cell and the integration process starts again. The droplet trajectory is traced until the first of the following conditions is met.

    a) droplet diameter diminishes to zero;
    b) droplet leaves through the exit of the calculation domain; or
    c) droplet hits the chamber wall where it evaporates.

A special treatment is required for tracking the droplet on a nonorthogonal grid. Figure 4.6-2 depicts a typical droplet trajectory and its inlet (IN) and exit (EX) cell boundary intersection locations.
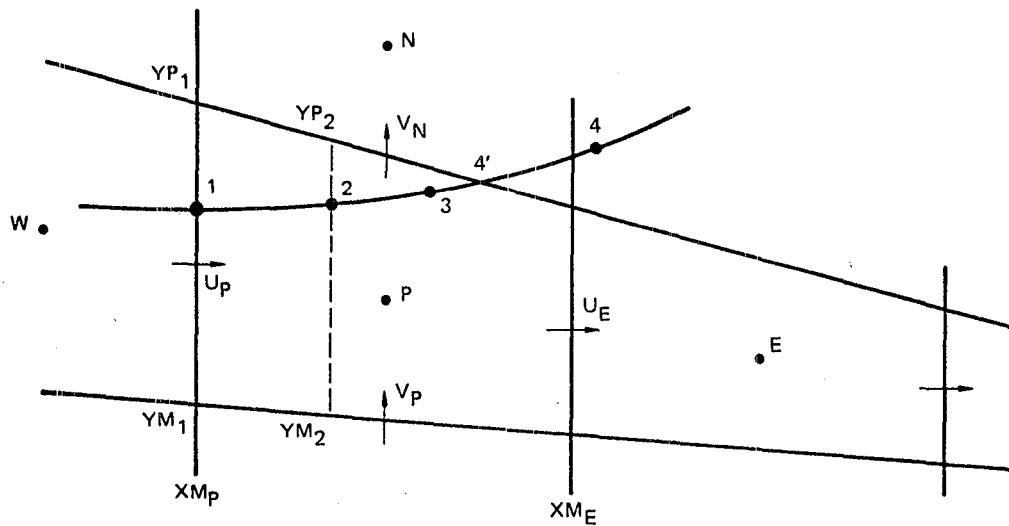
Figure 4.6-2. Droplet Tracking on Nonorthogonal Grid

In the case of orthogonal coordinates the cell boundaries XM_E, XM_P, YM_N, YM_P (Figure 4.6-2) were constant within the grid cell and independent on the droplet location. For nonorthogonal coordinates, however, at every integration step a continuous update of YM_P and YM_N as a function of x_z - droplet location is required.

Also the interpolation process of the Exit droplet position (point 4 in Figure 4.6-2) requires the solution of two algebraic equations viz:

- droplet trajectory equation; and
- grid cell face plane equation.

4.7   Interphase Transfer Source Terms

In the philosophy of the Eulerian-Lagrangean approach, the droplets are regarded as source of mass, momentum and energy to the conveying gaseous phase. The source terms are incorporated into the gas flow equations, providing the influence of the droplet spray on the gas velocity and temperature fields.

In each grid cell crossed by the droplet trajectory,appropriate interphase sources are calculated based on the droplet mass, momentum and energy difference between the inlet and the outlet from the cell.

4-31

The number of particles per unit time, which enter at port i and have an initial mass M_{dj}^{0} is given by:

$$M_{dji} = \dot{m}_d \, S_j \, Y_i \tag{4.6-7}$$

where $\dot{m}_d$ is the total droplet mass inflow rate, X_j is the fraction of droplet mass which enters at port j, and Y_i is the fraction of droplet mass with initial diameter D_i. The number flow rate of spherical droplets with initial diameter D_i, along a given trajectory is calculated as:

$$\dot{n}_y = \frac{6 \, \dot{m}_d \, X_j \, Y_i}{\pi \, \rho_d \, D_i^3} \tag{4.6-8}$$

where ρ_d is the droplet density.

This value is constant along a droplet trajectory, provided no droplet coalescence or shattering takes place.

Assuming the droplets are spherical, the continuity source term, $\Delta\dot{m}_d$, representing the net efflux rate of droplet mass to the gas phase, is given by:

$$\Delta\dot{m}_d = \frac{\pi}{6} \sum_i \sum_j \dot{n}_{ij} \left((\rho_d \, D^3)_{EX} - (\rho_d \, D^3)_{INL} \right) \tag{4.6-9}$$

where the summations are performed over all trajectories crossing the grid cell. The "EX" and "INL" subscripts refer to the droplet exit from and inlet into the control volume (Figure 4.6-2). The source terms for the remaining dependent variables ϕ (u, v, w, k, ε, $\tilde{h}$, m_j ...) are calculated from the following expression:

$$S_{INT,\phi} = \Delta\dot{m}_d \, (\bar{\phi}_d - \bar{\phi}) \tag{4.6-10}$$

where $\bar{\phi}_d$ and $\bar{\phi}$ represent average ϕ-property of the liquid and gas phase in the control volume, respectively. Note that the above formula can be conveniently linearized as:

$$SU_{INT,\phi} = \Delta m_d \cdot \phi_d$$

$$SP_{INT,\phi} = - \Delta m_d \tag{4.6-11}$$

With the assumption that the mass is transferred from liquid to the gaseous phase ($\dot{m}_d > 0$). A simple way to calculate droplet average property $\bar{\phi}_d$ is to take an average from the inlet $\phi_{d,INL}$ and exit $\phi_{d,EX}$ to the control volume and then weighted on all droplet sizes. Some of the droplet properties remain constant during the integration period and average $\bar{\phi}_d$ can be specified directly. These include:

$$\bar{\phi}_d = 1 \qquad\qquad , \text{ for } f \text{ and } m_{fu}$$

$$\bar{\phi}_d = Cp_d \cdot T_{sat} + H_{FU} , \text{ for } h$$

$$\bar{\phi}_d = 0 \qquad\qquad , \text{ for } k, \varepsilon \text{ and } m_{CO}$$

where Cp_d and H_{FU} are droplet specific heat, and droplet mass heat of combustion.

4.7.1 Interphase Momentum Transfer

There are two mechanisms of the momentum transfer between the liquid and vapor.

1) momentum transfer with the associated mass:
$$\Delta\dot{m} (\bar{u}_d - \bar{u}) \qquad\qquad\qquad (4.6\text{-}12)$$

2) frictional momentum transfer:
$$f_D (\bar{u}_d^2 - \bar{u}^2) \qquad\qquad\qquad (4.6\text{-}13)$$

The second mechanism has not been incorporated in the present version of the code and is planned to be included in the future calculations. Nonlinear characters of the friction terms requires special linearization practice for the momentum equation source terms. The linearization practice for these terms should be implemented in the following manner:

a) the source term can be expressed as:

$$S_u = Su^* + \left.\frac{\partial Su}{\partial u}\right|^* (u - u^*) =$$

$$f_D (\bar{u}_d^2 - \bar{u}^{*2}) - 2 f_D |\bar{u}^*| (\bar{u} - \bar{u}^*) \qquad\qquad (4.6\text{-}14)$$

b) appropriate source terms for the u-momentum equation should be added as follows:

$$SU_u = SU_u + f_D (\bar{u}_d^2 + 2|\bar{u}^*|\bar{u}^* - \bar{u}^{*2}) \qquad\qquad (4.6\text{-}15)$$

$$SP_u = SP_u - 2 f_D u^*$$

5. BOUNDARY CONDITIONS AND THEIR TREATMENT

5.1 Introduction

In order to completely specify the mathematical problem it is necessary to supply the conditions at the boundaries of the solution domain for all the dependent variables. These conditions are usually either specification of the value of the dependent variable at the boundary, or the value of the associated flux or a relation between the two.

Figure 5.1 presents an example of the computational domain and appropriate boundary conditions which may in general include:

1. inlet of gaseous or liquid species (fuel, air, steam, etc.);
2. exits plane;
3. center-lines and/or symmetry planes;
4. periodic boundary conditions; and
5. solid walls.
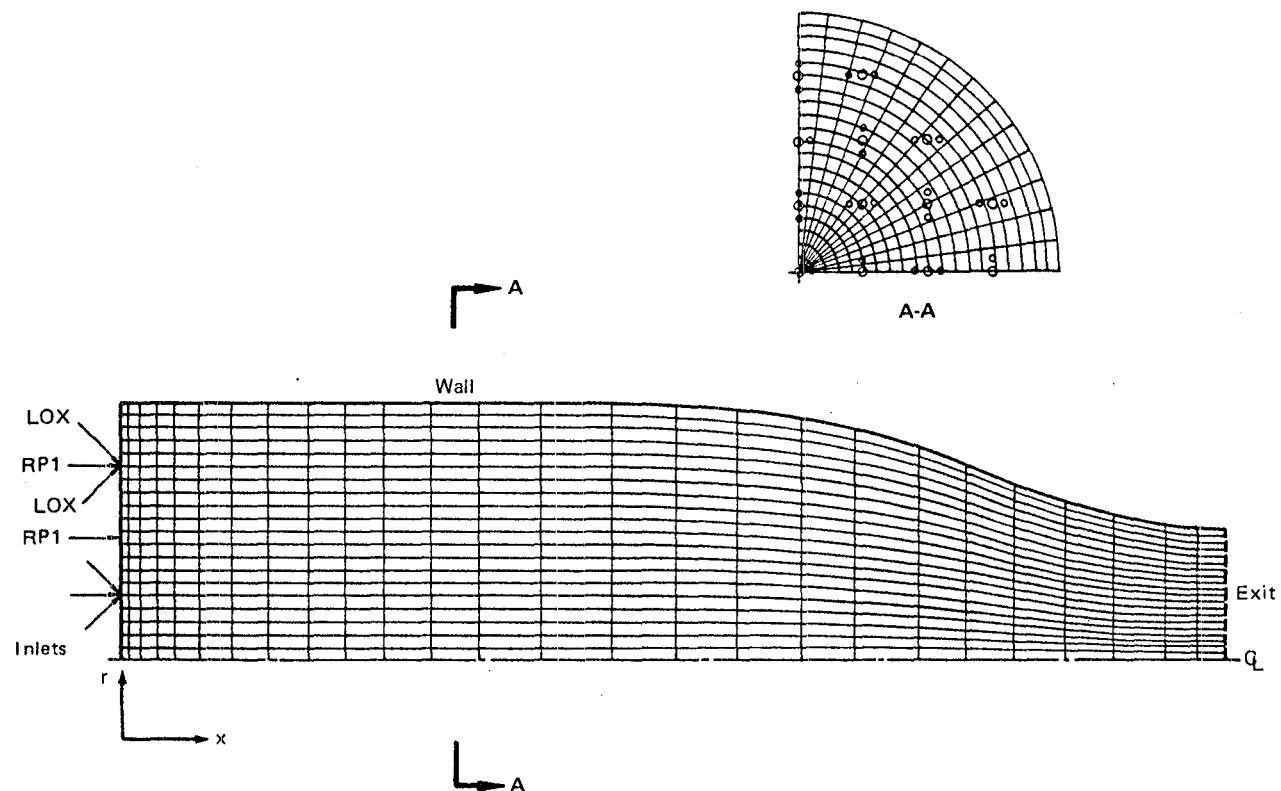
Figure 5.1. Computational Domain and Boundary Condition Specification

For each dependent variable, at all boundaries, appropriate modifications of the finite difference equation at the "near boundary" nodes is required. For most of the dependent variables the boundary conditions are implemented by modifying the source terms SU_ϕ and SP_ϕ of the finite difference equation:

$$\phi_P = \frac{\sum\limits_d a_d \, \phi_d + SU_\phi}{\sum\limits_d a_d - SP_\phi} \qquad (5.1-1)$$

These modification practices are discussed in the following sections.

5.2   Inlet With Specified Flow Rate

At the inlet the amount of incoming mass flow rate $\dot{m}_{IN}$ through the boundary cell face and the incoming ϕ_B property should be specified. In this case the finite-difference coefficient connecting the boundary node to its neighboring internal node is set to zero and then the SU_ϕ and SP_ϕ source terms are modified as:

$$SU_\phi = SU_\phi + \dot{m}_{IN} \, \phi_B \qquad (5.2-1)$$

$$SP_\phi = SP_\phi - \dot{m}_{IN} \qquad (5.2-2)$$

The pressure correction equation is not modified in this manner. A link coefficient with the boundary node is set to zero for p'-equations.

5.3   Symmetry Plane or Axis

At symmetry plane a zero mass flux $\dot{m}_{IN} = 0$ is assumed. The modification is implemented by setting the appropriate coefficient to zero (Figure 5.2) and no modification is required to the source terms.
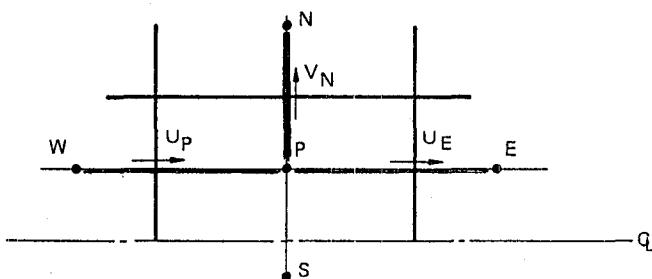

Figure 5.2. $a_s = 0$ at the Symmetry Plane

Gas phase injectors, or liquid spray injections with instantaneous evaporation assumption, are treated in a similar way. The liquid spray injection for which the Lagrangean droplet tracking is employed do not require specification boundary conditions in Eulerian meaning. Instead an appropriate initial droplet condition should be specified.

5.4   Exit Boundary

Where the fluid flows out of the calculation domain, information about most of the dependent variables is often not available. However, since it is the process occurring in the calculation domain that decide the values of the variables which the outgoing fluid will carry, information is not strictly required at such boundaries. To treat these boundaries, the boundary coefficients are simply set to zero.

If a fixed exit pressure boundary condition is specified, the velocity normal to the exit plane is solved for at the exit boundary and the pressure correction p' - link coefficient with the exit boundary is calculated. A specified pressure correction $p'_E = 0$ at the exit boundary is employed.

5.5   Periodic Boundary Conditions

The periodic (cyclic) boundary conditions appear in the circumferential direction if the two ends of the calculation domain in the z-direction join up with one another. This can occur in a polar-coordinate direction in which the whole angular extent from 0 to 360° is to be considered (Figure 5.3a), or when "repetition" is present in the flow pattern in the angular coordinate direction (Figure 5.3b).

The general rule is that whenever identical conditions are to be expected at z = 0 and z = last z, and finite flow is to be expected at that surface, then the boundaries are cyclic.

In this circumstance, the boundary conditions can be specified as follows:
$$\phi_{LB} = \phi_N \quad , \quad \phi_{HB} = \phi_1 \quad \text{and} \quad C_1^z = C_{HB}^z \quad (5.5-1)$$

where indices HB and LB denote High Boundary (k = N) and Low Boundary (k = 1), C^z is the convective flux in the z-direction.
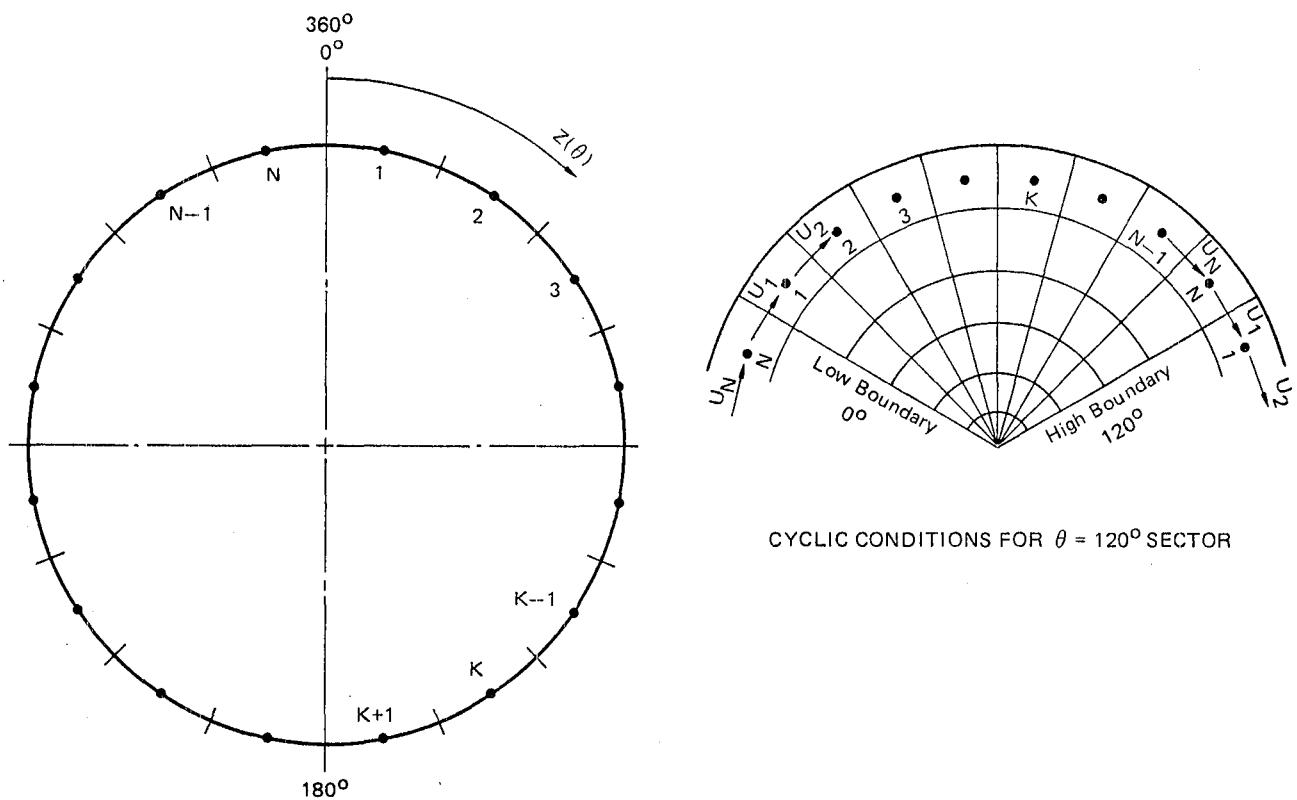
Figure 5.3. Grid Notation for Periodic Boundary Conditions in Z-Direction

5.6 Wall Boundaries

At the solid walls, the velocity normal to the wall and appropriate convective and diffusive fluxes are set to zero. The boundary conditions which can be easily specified at the solid walls (Figure 5.4) include:

$$V_B = 0, \tag{5.6-1}$$

$$\left. \frac{\partial \phi}{\partial y} \right|_B = 0 \qquad (\phi = f, \; m_{FU} \text{ and } m_{CO}) \tag{5.6-2}$$
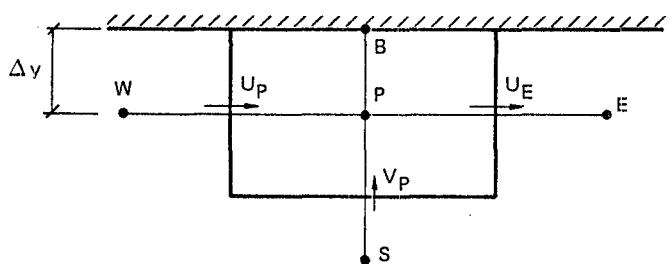
Figure 5.4. Grid Cell Adjacent to the Solid Wall

The boundary conditions for velocity components parallel to the wall; for k, ε and $\tilde{h}$ require special "near wall" treatment.

There are two important features that distinguish near-wall regions from other parts of the flow field. Firstly, there are steep gradients of most of the flow properties, and secondly, the turbulent Reynolds number is low so that the effects of molecular viscosity can influence the shear stresses, production dissipation and transport of turbulence energy.

The vigorous incorporation of these effects requires a prohibitively fine finite-difference grid in the vicinity of the wall.

An alternative approach, however, is available which bridges the near wall region and the outer edge of the viscous sublayer by using the "wall functions". These are described below.

5.6.1 Wall Functions

The wall functions described by Patankar and Spalding (Reference 55), Launder and Spalding (References 1, 56) and more recently by Launder (Reference 57) are derived from experimental and analytical knowledge of the one-dimensional Couette flow which exists near the wall. A semi-empirical universal function of nondimensional distance normal to the wall y^+, is:

$$y^+ \equiv \frac{\rho \; \delta y \cdot u_\tau}{\mu} \tag{5.6-3}$$

In the above definition δy is the distance normal to the wall (Figure 5.4) and u_τ is the "friction velocity" given by:

$$u_\tau = \left(\frac{\tau_w}{\rho}\right)^{1/2} \tag{5.6-4}$$

In the internal sublayer ($y^+ > 11.63$) the velocity variation may be described by a logarthmic relationship (see Schlichting (Reference 58)) i.e.:

$$\bar{u} = \frac{u_\tau}{\kappa} \ln (E y^+) \tag{5.6-5}$$

where $E = 9.793$ and $\kappa = 0.4187$ are experimentally determined constants.

In both the viscous ($y^+ \leq 11.63$) and internal ($y^+ > 11.63$) sublayers, the shear stress is calculated from the product of effective viscosity μ_{eff} and normal velocity gradient $\partial u / \partial y$, i.e.:

$$\tau_w = \mu_{eff} \frac{\partial \bar{u}}{\partial y} \tag{5.6-6}$$

where
$$\mu_{eff} = \begin{cases} \mu & \text{for } y^+ \leq 11.63 \\ \mu_{turb} & \text{for } y^+ > 11.63 \end{cases} \tag{5.6-7}$$

Near the wall, the transport equation for the turbulent kinetic energy, k, reduces to a balance between the local production and dissipation of k (References 1, 56) to give:

$$\mu_t \left(\frac{\partial \bar{u}}{\partial y} \right)^2 = \rho \varepsilon \tag{5.6-8}$$

The velocity gradient may be replaced from equation (5.6-6) and the dissipation rate from:

$$\mu_t = C_\mu \, \rho \, \frac{k^2}{\varepsilon} \tag{5.6-9}$$

to give:

$$\tau_w = C_\mu^{1/2} \, \rho \, k = \rho \, u_\tau^2 \tag{5.6-10}$$

Hence, it follows from equation (5.6-5)

$$\tau_w = \frac{\rho \, C_\mu^{1/4} \, k^{1/2} \, \bar{u}}{\frac{1}{\kappa} \, \ell n \, (Ey^+)} \tag{5.6-11}$$

5.6.2 Velocity Boundary Conditions

Equation (5.6-11) is introduced into the finite-difference equation (5.1-1) by setting the value of the link coefficient a_d (connecting point p with the wall node B) to zero, and adding to SP_u the term $\tau_w \cdot A_{wall}$ where A_{wall} is the cell wall area over which τ_w acts. For the velocity normal to the wall the same process is applied, but the normal shear stress is set to zero.

5.6.3 Turbulence Variables

Due to the steep velocity gradients near the solid walls the assumption of linear variation of $\bar{u}$ is inaccurate and can cause incorrect evaluation of the turbulence generation rate G. To overcome this, the generation term near the wall is written as

$$G_k = \tau_w \frac{\partial u}{\partial y} \tag{5.6-12}$$

where τ_s is evaluated according to equation (5.6-11). This is incorporated into the difference equation (5.1-1) by setting the link coefficient a_d to zero and modifying the source terms as follows:

$$SU_k = \tau_w \frac{\partial \bar{u}}{\partial y} \tag{5.6-13}$$

$$SP_k = - \frac{\rho^2 \, C_D k}{\tau_w} \frac{\partial \bar{u}}{\partial y} \tag{5.6-14}$$

The diffusion of the dissipation rate of turbulence at the wall is a little difficult to express. Instead of attempting to calculate Γ_{wall} for ε, use is made of the fact that the length scale ℓ varies linearly with distance in the neighborhood of a wall. Thus, the practice is to "fix" the value of ε at the near-wall grid point in accordance with:

$$\varepsilon = C_D^{\,3/4} \, k^{\,3/2} \, (\kappa \delta) \tag{5.6-15}$$

The fixing of ε (and similarly for other quantities) can be done by the use of the following expressions for SU_ε and SP_ε of the near-wall point:

$$SU_\varepsilon = 10^{10} \varepsilon \quad * $$

$$\text{and } SP_\varepsilon = - 10^{10} \tag{5.6-16}$$

When such large values of SU and SP are present, the actual value of a normal Γ_{wall} is immaterial.

---

*Instead of 10^{10}, any suitable large number may be used, as long as it is ensured that the other terms in the finite-difference equation are negligible compared to these two terms.

5.6.4 Stagnation Enthalpy

For turbulent flow, expressions have been developed, similar in form, to equation 5.6-11, in order to evaluate the heat flux $\dot{q}_w$ across the wall boundary layer; the one employed here is due to Jayatillaka (Reference 57) and writes:

$$\dot{q}_w = - \frac{\mu \, y^+}{\sigma_h} \left\{ \frac{1}{\kappa} \ell n \, (Ey^+) + P_h \right\}^{-1} \frac{dT_w}{dy} \qquad (5.6-17)$$

where $\frac{\partial T_w}{dy}$ is the normal temperature gradient. The term, P_h, expresses the contribution of the laminar sublayer to the total resistance and is calculated as:

$$P = 9 \left\{ \frac{\sigma_\ell}{\sigma_h} - 1 \right\} \left\{ \frac{\sigma_\ell}{\sigma_h} \right\}^{-1/4} \qquad (5.6-18)$$

where σ_c and σ_n are laminar and turbulent Prandtl numbers, respectively.

For laminar flow ($y^+ < 11.63$) the corresponding expression for the heat flux is:

$$\dot{q}_w = - \frac{\mu_\ell}{\sigma_\ell} \frac{d \, T_w}{dy} \qquad (5.6-19)$$

Equation (5.1-1) for h is modified by breaking the link between the near-wall nodes and adding to SU_h the term $\dot{q}_w \cdot A_{wall}$, where A_{wall} is the cell-wall area through which $\dot{q}_w$ is transferred.

5.7 Boundary Conditions for the Radiation Equations

A provision of zero gradient of net radiative heat fluxes at the calculation domain boundaries is provided as the default case. This is achieved by making relevant boundary link coefficients to zero. Other boundary specifications can be handled by the modifications of the near-boundary source terms. This is outlined below.

Making the boundary coefficient zero implies that $(\Gamma dR_X/dx)$ for the boundary cell surface is made zero. This can be seen to be equal to $-Q_X/2$ from equation 3.6-3.

Thus, the required source-term modification for the cell close to the boundary can be stated as the inclusion of $-Q_X/2$ for the boundary as an additional source term. For various particular cases, this will involve the following additional contributions to SU and SP.

Symmetry Plane

At a symmetry plane, Q_X is zero by definition. Hence no modification of SU and SP is needed.

Non-Reflecting Boundary

If the outgoing radiation leaves the calculation domain without reflection and if the incoming radiation, equal to, say L, is given, from the definitions of R_X and Q_X,

$$-Q_X/2 = L - R_X \tag{5.7-1}$$

Thus the additional SU should be L (which is given) and the additional SP should be -1.

Wall Boundary

If ε_W is the emissivity of the wall and E_W the black-body emissive power at the wall temperature, the flux leaving the wall, say L, is given by:

$$L = \varepsilon_W E_W + (1 - \varepsilon_W) K \tag{5.7-2}$$
$$\quad \text{emitted} \quad \text{reflected}$$

Again, via the definitions of Q_X and R_X, the following relation is obtained from equation (5.7-2):

$$-\frac{Q_X}{2} = \left(\frac{\varepsilon_W}{2 - \varepsilon_W}\right) E_W - \left(\frac{\varepsilon_W}{2 - \varepsilon_W}\right) R_X \tag{5.7-3}$$

Thus, $\{\varepsilon_W E_W/(2 - \varepsilon_W)\}$ becomes the additional SU while $\{-\varepsilon_W/(2 - \varepsilon_W)\}$ is the additional SP.

The y- and z-direction fluxes are treated in a similar manner. It should, however, be remarked that for the radial direction the additional source term for the y-direction flux is $(-rQ_y/2)$, where r is the radius of the boundary surface.

6. NOMENCLATURE

$A_W, A_E, \ldots$ — Area of the grid cell (W-face, E-face, ...)

a — Absorption coefficient for radiation

$a_E, a_W, \ldots$ — Finite difference link coefficient (E-east, W-west, N-north, ...)

a_{ox} — Oxygen mass fraction in oxidizer

a_j — Polynomian coefficient for cp-calculation

B — Eddy-Break-Up model constant

b_j — Polynomian coefficient for cp-calculation

C — Convective flux

C_1, C_2, C_D — Turbulence model constants

C_p — Specific heat of mixture at constant pressure

c_j — Polynomian coefficient for cp-calculation

D — Droplet diameter

DU, DV, DW — Pressure-difference coefficients

d_j — Polynomian coefficient for cp-calculation

E — Activation energy in the Arrhenius reaction rate law (Chapter 3.7); or

Black body emissive power (Chapter 3.6); or

A constant in the law of the wall (Chapter 5)

f — Mixture fraction

G_k — Generation rate of turbulence energy

g — Concentration fluctuation

H_j — Heat of combustion for j-th species

$\tilde{h}$ — Stagnation enthalpy

I — False inertia term (Chapter 4.5); or

Radiation flux in the positive x-direction (Chapter 3.6)

J — Radiation flux in the negative x-direction

K — Radiation flux in the positive r-direction

k	- Kinetic energy of turbulence
L	- Radiation flux in the negative r-direction
M	- Mixture molecular weight (Chapter 3.3); or
	Radiation flux in the positive z-direction (Chapter 3.6); or
	Mass of the control volume (Chapter 4.3)
M_j	- Molecular weight of species j
m_j	- Mass fraction of species j
m	- Coefficient in hydrocarbon composition ($C_n H_m$) specification
N	- Radiation flux in the negative z-direction
NS	- Number of species participating in the mixture composition
n	- Coefficient in hydrocarbon composition ($C_n H_m$) specification
P	- Resistance of the laminar sublayer (Chapter 5.6); or
	Pre-exponential factor in Arrhenius reaction rate expression (Chapter 3.7)
p	- Pressure
p'	- Pressure correction
Q_x, Q_y, Q_z	- Net radiative heat fluxes in the x, y and z (or θ) directions
R_j	- Mass rate of creation of species j by chemical reaction
R	- Universal gas constant
R_x, R_y, R_z	- Composite radiation fluxes (dependent variables) in the x, y, z (or θ) directions
r	- Distance from axis of symmetry
S	- Source term
SU, SP	- Parts of linearized source term
s	- Mass ratio of stoichiometric osidant/fuel proportions (Chapter 3.7); or
	- Radiation scattering coefficient (Chapter 3.6)
T	- Absolute temperature
t	- Time

u, v, w	- Velocity components in the x, y and z (or θ) directions
U	- Velocity vector
W	- Angular velocity ($W \equiv rw$)
x, y, z	- Coordinate distances
y^+	- Dimensionless distance from the wall

Greek Symbols

α	- Relaxation factor
γ	$\equiv m_{fu} - m_{ox}/s$
Γ	- Diffusion coefficient
$\Delta x, \Delta y, \Delta z$	- x-direction, y-direction and θ (or z) direction lengths of a control volume
$\delta x, \delta y, \delta z$	- x-, y- and z-direction distances between the node points
ε	- The dissipation rate of turbulence
ε_W	- Wall emissivity
θ	- Coordinate distance
κ	- Von Karman constant
μ	- Viscosity
ρ	- Density
σ	- Laminar Prandtl/Schmidt number (Chapter 3.8); or Stefan-Bolzman constant (Chapter 3.6)
ϕ	- The general dependent variable
Ω	- Spherical angle

Subscripts

A	- Air inlet
d	- Droplet
eff	- Effective value
E	- East side (x^+) neighbor
EBU	- Eddy-break-up
fu	- Fuel

F	- Fuel inlet
H	- High size (z^+) neighbor
$\tilde{h}$	- Stagnation enthalpy
int	- Interphase value
j	- Species j
k	- Kinetic energy of turbulence
L	- Low size (z^-) neighbor
l	- liquid
ℓ	- Laminar
N	- North side (y^+) neighbor
ox	- Oxygen
pr	- Products
stoich	- Stoichimetric
S	- South side (y^-) neighbor
t	- Turbulent
v	- Vapour
W	- West side (x^-) neighbor

7. REFERENCES

1. Launder B.E. and Spalding D.B., "Mathematical Models of Turbulence", Academic Press, London and New York, 1972.

2. Bradshaw P., "Turbulence", Topics in Applied Physics, Volume 12, Springer Verlag, Berlin, New York, 1978.

3. Launder B.E. and Spalding D.B., "The Numerical Computation of Turbulent Flow", Comp. Meth. in Applied Mech. and Engr., Vol. 3, 1974, p 269.

4. Hottel H.C. and Sarofim A.F., "Radiative Heat Transfer", McGraw Hill, New York, 1967.

5. Howell J.R., "Application of Monte-Carlo to Heat Transfer Problems", Advances in Heat Transfer, Edited by Irvine and Hartnett, Vol. 5, Academic Press, New York, 1968.

6. Lockwood F.C. and Shah N.G., "A New Radiation Solution Method for Incorporation in General Combustion Prediction Procedures", Eighteenth Symposium (International) on Combustion, The Combustion Institute, Pittsburgh, 1981.

7. Schuster A., "Astrophysical Journal", Vol. 21, pp 1 - 22, 1905.

8. Hamaker H.C., "Radiation and Heat Conduction in Light-Scattering Material", Philips Research Report, Vol. 2, pp 55 - 67, p. 103, p. 112, p. 420, 1947.

9. Chandrasekhar S., "Radiative Transfer", Dover Publications, New York, 1960.

10. Lockwood F.C. and Spalding D.B., "Predictions of a Turbulent Reacting Duct Flow with Significant Radiation", Thermodynamic Session, Proc. Colloques d'Evian de la Societe Francaise de Physique, May 1981.

11.   Spalding D.B., "Concentration Fluctuations in a Round Turbulent Free
        Jet", Chem. Eng. Sci., 26, pp 95-107, 1971.

12.   Spalding D.B., "Mixing and Chemical Reaction in Steady Confined
        Turbulent Flame", Proc. 13th Symposium (International) on Combustion,
        pp 649-658, The Combustion Institute, 1970.

13.   Elghobashi S.E. and Pun W.M., "A Theoretical and Experimental Study
        of Turbulent Diffusion Flames in Cylindrical Furnaces", 15th International
        Symposium on Combustion, The Combustion Institute, Pittsburgh, pp 1353 -
        1365, 1974.

14.   Magnussen B.F. and Hjertager B.M., "On Mathematical Modeling of Turbulent
        Combustion with Special Emphasis on Soot Formation and Combustion", 16th
        Symposium (International) on Combustion, The Combustion Institute,
        pp 719-729, 1976.

15.   Soo S.L., "Fluid Dynamics of Multiphase Systems", Blaisdell Publ. Co.,
        1967.

16.   Ingebo R.D., "Drag Coefficient for Droplets and Solid Spheres in Clouds
        Accelerating in Airstreams", NACA Report TN-3762, 1956.

17.   Crowe C.T. and Pratt D.T., "Analysis of the Flow Field in Cyclone
        Separators", Computers and Fluids, Vol. 2, 1970.

18.   Wallis G.B., "One-Dimensional Two-Phase Flow", McGraw Hill, 1969.

19.   Bailey G.H., Slater I.W. and Eisenklam P., "Dynamic Equations and
        Solutions for Particles Undergoing Mass Transfer", Brit. Chem. Eng.,
        Vol. 15, NO. 7, p 912, 1970.

20.   Crowe C.T., Sharma M.P. and Stock D.E., "The Particle-Source-In Cell
        (PSI-Cell) Model for Gas Droplet Flows", ASME, Journal of Fluids
        Engineering, June 1977, pp 325-332.

21. Grzegolka K., Przekwas A.J. and Wanik A., "Prediction of Pulverized Coal Combustion in Combustion Chambers", ASME Meeting on Combustion and Fluid Flows, Boulder, Colorado, 1981.

22. Przekwas A.J., Singhal A.K. and Tam L.T., "Modeling of Two-Phase Reactive Flows in Swirl Combustion Chambers" to be presented at International Symposium on Gas-Solid Flows, ASME Spring Meeting, New Orleans, Feb. 11 - 17, 1984.

23. Kanuray A.M., "Introduction to Combustion Phenomena", Gordon and Beach, 1975.

24. Chigier N.A., "The Atomization and Burning of Liquid Fuel Spray", Progress in Energy and Combustion Science, Vol. 2, 97, 1976.

25. Faeth G.M., "Current Status of Droplet and Liquid Combustion", Progress in Energy and Combustion Science, Vol. 3, 191, 1977.

26. Bird R.B., Stewart W.E. and Lightfoot E.N., "Transport Phenomena", Jon Willey, New York, 1960.

27. Ranz W.E. and Marshall W.R., Jr., "Evaporation from Drops", Chemical Engineering Progress, Vol. 48, No. 3 and No. 4, 1952.

28. Patankar S.V. and Spalding D.B., "A Calculation Procedure for Heat, Mass and Momentum Transfer in Three-Dimensional Parabolic Flows", International Journal of Heat and Mass Transfer, Vol. 15, pp 1787 - 1806, Pergamon Press, 1972.

29. Patankar S.V., "Numerical Heat Transfer and Fluid Flow", McGraw Hill, 1980.

30. Harlow F.H. and Nakayama P.I., "Transport of Turbulence Energy Decay Rate", Los Alamos Sci. Lab., University of California, LA-3854, Feb. 1968.

31. Launder B.E. and Spalding D.B., "The Numerical Computation of Turbulent Flows", Computer Methods in Applied Mechanics & Engr., Vol. 3, pp 169 - 289, 1974.

32. Spalding D.B., "A General Computer Program for Fluid Flow, Heat Transfer and Chemical-Reaction Processes", Paper presented at Inter. FEM-Congress, Baden-Baden, Germany, 1980.

33. Hung T.K. and Brown T.D., "An Implicit Finite-Difference Method for Solving the Navier-Stokes Equations Using Non-Orthogonal Curvilinear Co-Ordinates", J. Computational Physics, Vol. 23, p 343, 1977.

34. Pope S.P., "The Calculation of Turbulent Recirculating Flows in General Coordinates", J. Computational Physics, Vol. 26, p 197, 1978.

35. Gosman A.D. and Jones R.J.R., "Computer Analysis of Fuel-Air Mixing in Direct Injection Engines", SAE Ppaer 800091, 1980.

36. Benjamin S.F., Weaving J.H., Glynn D.R., Markatos N.C. and Spalding D.B., "Development of a Mathematical Model of Flow, Heat Transfer and Combustion in a Stratified Charge Engine", Mechanical Engineering Stratified Charge Automotive Engine Conference Ppaer, C403/80, 1980, pp 91 - 99.

37. Spalding D.B., "A Novel Finite Difference Formulation for Differential Expressions Involving Both First and Second Derivatives", Int. J. Num. Meth. in Engineering, Vol. 4, 551, 1972.

38. Roache P.J., "Computational Fluid Dynamics", Hermossa Publ., 1974.

39. Chorin A.J., "Numerical Solution of the Navier-Stokes Equations", Mathematics of Computation, Vol. 22, p 745, 1968.

40. Varga R.S., "Matrix Iterative Analysis", Prentice Hall, 1962.

41. Reid J.K., "Large Sparce Sets of Linear Equations", Academic Press, London, 1970.

42.   Wachpress E.L., "Iterative Solution of Elliptic Systems", Prentice Hall, Enelwood Cliffs, New Jersey, 1966.

43.   Paceman D.W. and Rachford Jr., H.H., "The Numerical Solution of Parabolic and Elliptic Differential Equations", J. Soc. Indust. Appl. Math., Vol. 3, pp 28-41, 1955.

44.   Stone H.L., "Iterative Solution of Implicit Approximation of Multidimensional Partial Differential Equations", SIAM J. Num. Annual., Vol. 5, 1968.

45.   Gosman A.D., Tsui Y.Y. and Watkins A.P., "Calculation of Three-Dimensional Air Motion in Model Engines", SAE Ppaer No. 840229, 1984.

46.   DuPont T., Kendall R.D. and Rachford M.D., "An Approximate Factorization Procedure for Solving Self-Adjoint Elliptic Difference Equation", SIAM J. Num. Anal., Vol. 5, 1968.

47.   Saylor P.E., "Second Order Strongly Implicit Symmetric Factorization Method for the Solution of Elliptic Difference Equations", SIAM J. Num. Anal., Vol. 71, 1974.

48.   Schnieder G.E. and Zedan M., "A Modified SIP for the Numerical Solution of Field Problems", Numerical Heat Transfer, Vol. 4, 1981.

49.   Przekwas A.J., "Whole Field Solution Method Elliptic Difference Equations with General Boundary Conditions", Under preparation for submission to Numerical Heat Transfer.

50.   Mongia H.C. and Reynolds R.S., "Combustor Design Criteria Validation", Vol. 3, Air Research Mfg. Co., Report prepared for US ARTL, 1978.

51.   Faeth B., Aggarwal S.K. and Sirignano W.A., "Flame Propagation Through an Air-Fuel Spray Mixture with Transient Droplet Vaporization", Combustion and Flame, Vol. 39, p 149, 1980.

52. Aggarwal A.K., Fix G.J., Lee D.N. and Sirignano W.A., "Numerical Optimization Studies of Axisymmetric Unsteady Sprays", Journal Computational Physics, Vol. 50, pp 101-115, 1983.

53. Gosman A.D. and Jones R.J.R., "Computer Analysis of Fuel-Air Mixing in Direct Injection Engines", SAE Paper 800091, 1981.

54. Abbas A.S., Koussa S.S. and Lockwood F.C., "The Prediction of the Particle Ladden Gas Flows", 18th Symposium (International) on Combustion, The Combustion Institute, 1981.

55. Patankar S.V. and Spalding D.B., "A Calculation Procedure for Heat, Mass and Momentum Transfer in Parabolic Flows", Int. J. Heat Mass Transfer, Vol. 15, pp 1787-1806, 1972.

56. Launder B.E. and Spalding D.B., "The Numerical Computations of Turbulent Flows", Computer Methods in Appl. Mech. and Engineering, Vol. 3, 1974.

57. Chieng C.C. and Launder B.E., "On the Calculation of Turbulent Heat Transport Downstream from an Abrupt Expansion", Numerical Heat Transfer, Vol. 3, pp 189-207, 1980.

58. Schlichting H., "Boundary Layer Theory", McGraw Hill, 1968, (6th Edition).

59. Jayatillaka C.V.L., "The Influence of Prandtl Number and Surface Roughness on the Resistance of the Laminar Sub-Layer to Momentum and Heat Transfer", Progress in Heat and Mass Transfer, Vol. 1, Pergamon Press, London, 1969.

60. Spalding, D.B., "A General Purpose Computer Program for Multi-Dimensional One- and Two-Phase Flow," Mathematics and Computers in Simulation, North Holland Press, Vol XXIII, pp. 267-276, 1981.

61.   Singhal A.K., Keeton L.W., Przekwas A.J., Weems J.S., Spalding D.B.,
       and Srikantiah G., "ATHOS - A Computer Program for Thermal Hydraulics
       of Steam Generators"
       Volume 1: Mathematical and Physical Models
       Volume 2: Programmer's Manual
       Volume 3: User's Manual
       Volume 4: Code Verification Applications.

End of Document